

“Any intelligent fool can make things bigger, more complex, and more violent. It takes a touch of genius...and lot of courage...to move in the opposite direction”

Albert Einstein
The Listener 54 (1955)

University of Alberta

Temperature dependence of the piezoelectric shear coefficient of PMN-PT,
LiNbO₃ and PZT transducers

by

Syed Asad Manzoor Bukhari

A thesis submitted to the Faculty of Graduate Studies and Research
in partial fulfillment of the requirements for the degree of

Master of Science

Department of Physics

© Syed Asad Manzoor Bukhari
Spring 2014
Edmonton, Alberta

Permission is hereby granted to the University of Alberta Libraries to reproduce single copies of this thesis and to lend or sell such copies for private, scholarly or scientific research purposes only. Where the thesis is converted to, or otherwise made available in digital form, the University of Alberta will advise potential users of the thesis of these terms.

The author reserves all other publication and other rights in association with the copyright in the thesis and, except as herein before provided, neither the thesis nor any substantial portion thereof may be printed or otherwise reproduced in any material form whatsoever without the author's prior written permission.

Abstract

Piezoelectric transducers are widely used as sensitive detectors of stress and to generate nanometer scale displacements. However, their piezoelectric coefficients often decrease substantially at cryogenic temperatures, limiting their performance in, e.g., low temperature STMs (scanning tunneling microscopes), biomedical imaging and space applications. Its important these days to understand the behavior of sensors and actuators at low temperatures because of their use at these temperatures. We have recently used PZT (lead zirconate titanate) shear transducers to measure the elastic modulus of solid ^4He at very low strains and to plastically deform the helium at high strains. From our elastic measurements, we inferred a shear piezoelectric coefficient $d_{15} = 1.0 \times 10^{-10}$ m/V below 1 K. This is about 6 times smaller than the room temperature value for PZT and comparable to d_{15} for single crystal LiNbO_3 transducers (7.0×10^{-11} m/V). We have now developed a capacitive technique and have directly measured the temperature dependence of d_{15} for ceramic (PZT) and single crystal LiNbO_3 and PMN-PT (lead magnesium niobium-lead titanate) shear transducers. PMN-PT has an extremely large d_{15} at room temperature (4.0×10^{-9} m/V) but it decreases rapidly below 100K. LiNbO_3 has the smallest room temperature d_{15} , but it is nearly temperature independent. At 4 K,

these three types of transducers d_{15} have similar piezoelectric shear coefficients.

Acknowledgements

I am very thankful to my supervisor Prof. John Beamish who guided me throughout of my degree as an ideal mentor. I acknowledge the useful discussions with my committee members Prof. John Davis, Prof. Frank Marsiglio and other faculty members in department of Physics. Thanks to Mr Shahid ul Islam for helping me in acquiring data, and maintaining our low temperature lab. I am thankful to Don Mullin, Greg Popowich, Steve Rogers, Paul Zimmermann, Dave Fortin, Devon Bizuk and other technical staff for their useful technical support. Special thanks to Sarah Derr, Sharon Morsink, Caroyln Steinborn, Suzette Chan, Patty Chu, Sandra Hamilton, and Linda Jacklin in the physics office. I also appreciate our collaborators in ENS, Paris. Special thanks to Ariel Haziot, Xavier Rojas and Sebastien Balibar. I would like to thank to my friends Asif, Tayyaba, Amna, Aatif, Shah Nawaz, Nadia, Jamil, Saeed, Peter, Scott, Joe, Jacob, Yikai, Logan, Burkhard, Junaid, Faheem, Hyder, Touqeer, and Zain who really helped me during the whole period of my studies here at U of A. It would have never been possible without the help and useful guidance of my parents, family and friends.

Contents

1	Introduction	1
1.1	Piezoelectric strain constant (d)	3
1.2	Piezoelectric voltage constant (g)	4
1.3	Electromechanical coupling coefficient (k)	4
1.4	Acoustic impedance (Z)	5
1.5	The mechanical quality factor (Q_M)	5
1.6	Motivation for current work	6
2	Literature review and background	9
2.1	Historical background-piezoelectricity	9
2.2	Paraelectricity, ferro-electricity, and piezoelectricity	11
2.3	Piezoelectric effect in single crystals	14
2.3.1	Single crystal LiNbO_3	20
2.3.2	Single Crystal PMN-PT	25
2.4	Polycrystalline PZT	33
2.5	Review of experimental methods	38
3	Experimental Techniques	46
3.1	Cryogenics and low temperature	46
3.2	Thermometry	48
3.3	Pressure measurements and leak-testing	48
3.4	Experimental design for measuring d_{15}	50

3.4.1	Mathematical formalism and measurements	52
4	Results	60
4.1	PZT polycrystalline ceramic shear transducers	60
4.2	Poled single crystals of PMN-PT	69
4.3	Single crystal LiNbO ₃	78
4.4	Conclusions	87
5	Summary	89
5.1	Summary of lithium niobate	89
5.2	Summary for PMN-PT	90
5.3	Summary of PZT	91
5.4	Future directions	92

List of Tables

2.1	3-D array representing d_{ijk}	17
2.2	3-D array of symmetrized d_{ijk}	19
2.3	Observed values of piezoelectric coefficients for different temperatures	45

List of Figures

1.1	Piezoelectricity as a result of net dipole moment	2
1.2	The simplest example to demonstrate piezoelectricity	3
2.1	Single crystals domains, domain walls and polarization	12
2.2	Ceramic polycrystalline PZT, grains, dipoles and orientations . .	13
2.3	Transformation of axes	16
2.4	Single crystal LiNbO ₃	21
2.5	Phase transformation for LiNbO ₃ single crystals	22
2.6	Rotated axes and dimensional notations of LiNbO ₃ single crystals	24
2.7	MPB with other phases above and below the boundary	28
2.8	Temperature dependence of d_{15} for single crystals of PMN-PT .	30
2.9	Temperature dependence of d_{13} for PMN-PT from room tem- perature to liquid nitrogen temperature	32
2.10	PZT transducer modes	34
2.11	PZT phase diagram	36
2.12	Temperature dependence of PZT-4, 5A and 5H type transducers	39
2.13	Resonance and antiresonance	42
2.14	Temperature dependence of piezoelectric coefficients for lithium niobate	43
2.15	Lever-fulcrum technique to measure piezoelectric moduli	44
3.1	OFHC bracket attached with the 1K pot	47
3.2	Thermometers, heaters, 10 pin connectors and controllers	49

3.3	Schematic of the brass jig for d_{15} measurement	51
3.4	Step wise construction of the JIG for d_{15} measurement	53
3.5	Change of capacitance in a parallel plate capacitor	54
3.6	Schematic diagram of piezoelectric coefficients measurements	56
3.7	Schematic of capacitance-transducer set up	57
4.1	PZT-5A type shear transducer	61
4.2	PZT-5A capacitance vs. voltage	62
4.3	PZT-5A: calculating the average capacitance	63
4.4	Temperature dependence of PZT-5A type shear transducer	64
4.5	Temperature dependence of PZT-5A: linear fit of data	66
4.6	Hysteresis behavior of PZT at 1.4 K	67
4.7	Hysteresis behavior of PZT at 1.8 K	68
4.8	PMN-PT single crystals: temperature dependence of d_{15}	70
4.9	PMN-PT single crystals: capacitance vs. voltage at lowest temperature	71
4.10	PMN-PT single crystals: capacitance vs. voltage at 4 K	72
4.11	PMN-PT single crystals: capacitance vs. voltage at LN ₂ temperature	73
4.12	PMN-PT single crystals: capacitance vs. voltage at 100 K	74
4.13	PMN-PT single crystals: capacitance vs. voltage at 152 K	75
4.14	PMN-PT single crystals: capacitance vs. voltage at 200 K	76
4.15	PMN-PT single crystals: capacitance vs. voltage at 240 K	77
4.16	LiNbO ₃ single crystals:Temperature dependence of d_{15}	80
4.17	LiNbO ₃ single crystals: capacitance vs. voltage for lithium niobate at 1.3 K for ± 20 volts	81
4.18	LiNbO ₃ single crystals: capacitance vs. voltage for lithium niobate at 1.3 K for ± 150 V	82
4.19	LiNbO ₃ single crystals: capacitance vs. voltage for lithium niobate at 4 K	83

4.20	LiNbO ₃ single crystals: capacitance vs. voltage for lithium niobate at LN ₂ temperature	84
4.21	Comparison of temperature dependence of PZT, PMN-PT and lithium niobate	85
4.22	Comparison of temperature dependence of PZT, PMN-PT and lithium niobate with Log(d ₁₅	86

List of Abbreviations

List of commonly used abbreviations

PZT	Lead zirconate titanate
PMN-PT	Lead magnesium niobium-Lead titanate
IRE	Institute of Radio Standards
LVDT	Linear variable differential transformer
MPB	Metamorphic phase boundary
OFHC	Oxygen free high conductivity copper

Chapter 1

Introduction

Piezoelectric phenomena have been a multidisciplinary topic of interest because of their diverse applications in physics, chemistry, biosciences and engineering. Because of their diverse practical aspects, their fundamental properties need to be understood. Many research groups are now actively involved in studying these transducers in different sizes and shapes with a variety of different available materials depending on the required applications.

When a current flows through a single loop of wire, a magnetic field exists around the loop and generates a magnetic dipole having direction determined by the right hand rule. Similarly, permanent magnets exhibit permanent magnetic dipoles with north and south poles. In electrostatics, a partial electric charge appears at one side of atom or molecule which induces equal amount of negative charge on the other side because of electrostatic attraction which is at a smaller distance (atomic scale) from the positive charge. This distribution of positive and negative charges of equal magnitude and opposite polarity creates electric dipoles. The product of the magnitude of the charge and the separation between two charges is called the electric dipole moment. These dipoles are vectors and, when added, give a net polarization to a ferroelectric material. If we consider the crystal symmetry then we can clearly conclude that the crystals having center of symmetry cannot have a net polarization so they cannot

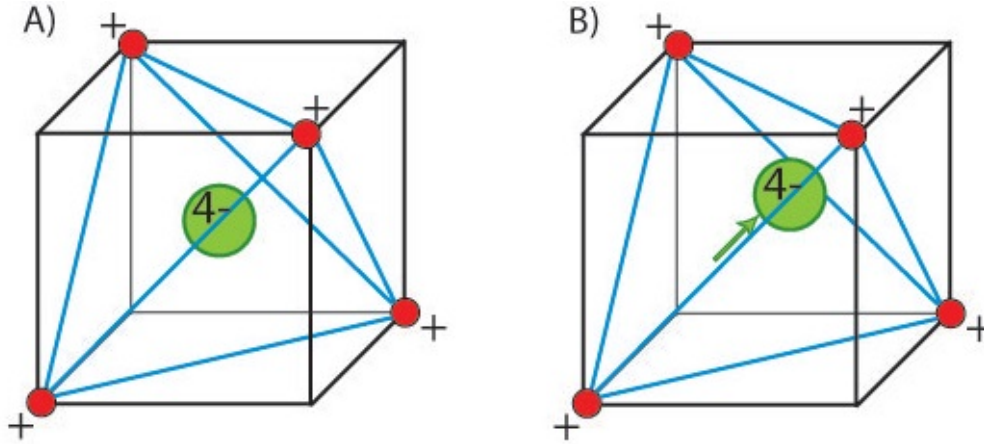


Figure 1.1: There is no net polarization in structure A and there is a finite polarization in B just because the location of the central charge is mobile which means only B would be piezoelectric [1].

be piezoelectric. The ferroelectric crystal must be non-centrosymmetric. In Fig. 1.1, there is no net displacement in A and the electric dipole moment is zero meaning no piezoelectric effect would be observed. However the central charge is displaced in B so there is a net dipole moment for this lattice and hence a macroscopic polarization corresponding to a bulk piezoelectric transducer. This suggests that the central atom should be displaced by a distance in order to get a net electric polarization leading to ferroelectric behavior.

When a mechanical stress is applied to a certain class of materials, a charge will be accumulated at its surface. This induced charge is proportional to the mechanical stress applied and will cause an electric field between the two surfaces of the material. This is called the piezoelectric effect. Piezo is a Greek word meaning pressure. So producing electricity with pressure is called piezoelectricity. This effect was first discovered in quartz by Pierre and Jacques Curie in 1880. The inverse of this mechanism is also true, i.e. when an electric potential is applied across a bar of piezoelectric material, it forces the bar to bend/deform under the applied voltage. This deformation or bending will

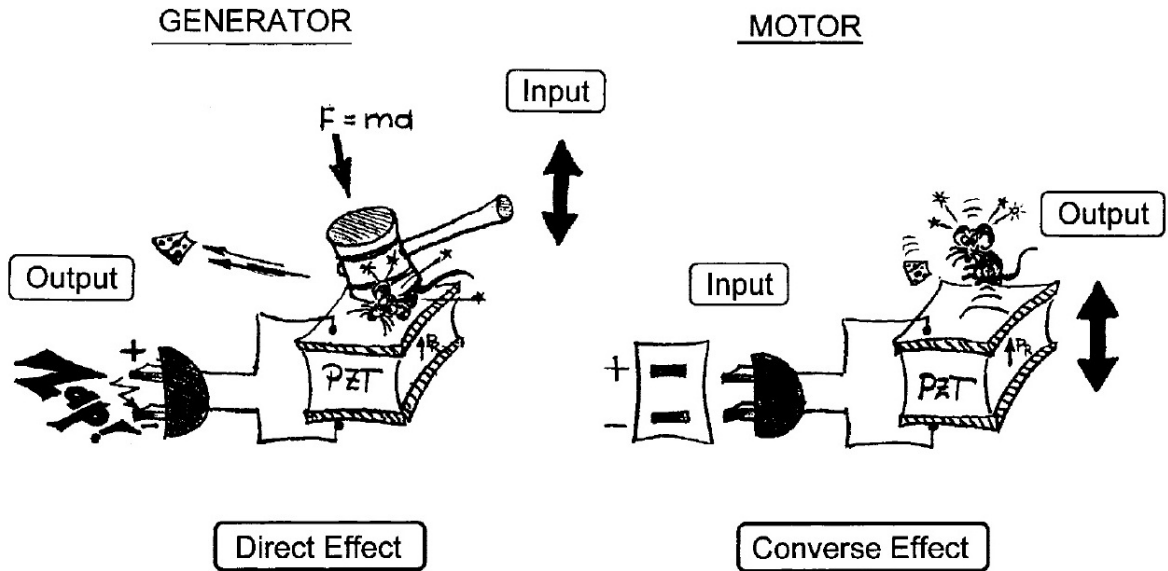


Figure 1.2: The cartoon shows how a hammer will produce electricity and how a mouse will feel the distortion produced in PZT by an applied electric field [3].

generate a disturbance in the medium (shear or compressional wave). A very simple example to understand the direct and converse piezoelectric effects is given in Fig. 1.2. These fascinating effects make it possible to fabricate various devices like transducers, actuators, surface acoustic wave devices, frequency control devices, etc. with single crystal and polycrystalline piezoelectric materials [2].

We now discuss briefly a list of important parameters to be remembered when we discuss designing piezoelectric transducers. These points are summarized as the characteristics of the piezoelectric materials.

1.1 Piezoelectric strain constant (d)

Let “ X ” be the displacement of the transducer under an applied voltage “ V ” then the ratio of “ X ” to “ V ” gives us the piezoelectric strain constant “ d ”, measured in units (m/V)

$$d = \frac{X}{V}. \tag{1.1}$$

For most piezoelectric transducers, we are interested to study three independent strain coefficients which are named as “ d_{33} ”, “ d_{31} ”, and “ d_{15} ” [4]. A large value of these “ d_{ij} ” means a large mechanical displacement which is what we are looking to make a better actuator. For “ d_{33} ”, the force is applied in the direction of polarization or the transducer is compressed in the same direction in which polarization charge accumulates. However, for “ d_{31} ”, the applied force is at right angle to the direction of the polarization. The shear strain coefficient “ d_{15} ” is obtained when the charge is induced at electrodes which are perpendicular to the direction of the polarization. This represents a pure shear mode and it will be the major topic of discussion in following chapters.

1.2 Piezoelectric voltage constant (g)

This figure of merit is important for a piezoelectric transducer which is to be used as a sensor. It gives us the ratio of the induced electric field “ E ” to the applied stress “ S ”

$$g = \frac{E}{S} \quad (1.2)$$

in units (V.m/N).

1.3 Electromechanical coupling coefficient (k)

A dimensionless number k, which is sometimes very important in defining polarization and vibration of the transducers, can be defined as the ability of the piezo transducer to transform the electrical energy into mechanical energy and vice versa.

$$k = \sqrt{\frac{E_{(EES)}}{E_{(MEI)}}} \quad (1.3)$$

or

$$\sqrt{\frac{E_{(MES)}}{E_{(EEI)}}} \quad (1.4)$$

where $E_{(EES)}$ represents the stored electrical energy, $E_{(MEI)}$ the input mechanical energy, $E_{(MES)}$ stored mechanical energy and $E_{(EEI)}$ is input electrical energy.

1.4 Acoustic impedance (Z)

The product of density of a material and its acoustic velocity gives the acoustic impedance ($\text{kg/m}^2 \text{ s}$). This is a useful parameter in determining the transmission and reflection of sound waves at the boundary between the two different piezoelectric materials, usually a backing and a matching layer which is used in designing imaging equipment in medical ultrasound technology. If ρ is the density of a material and v is the velocity of the sound wave propagating through it then,

$$Z = \rho v. \quad (1.5)$$

1.5 The mechanical quality factor (Q_M)

The mechanical quality factor Q_M is the ratio of the energy stored in an oscillatory system to the energy lost by the system during one oscillation cycle. High quality factor means lower loss of energy in the system per unit cycle which characterizes the sharpness of the electromechanical spectrum. The sharper the resonance peak, the smaller loss and higher the quality factor. Mathematically it can be expressed as,

$$Q_M = \frac{f_r}{\Delta f} \quad (1.6)$$

where f_r is the resonant frequency, Δf the half-power bandwidth i.e. qualitative measure of the full-width at half-maximum (FWHM) of intensity vs. frequency relation. Its a dimensionless number [4].

These specific characteristics of piezoelectric transducers are very useful in designing an actuator or a sensor. These are general characteristics independent of the the crystal structures of the materials however these merit points vary drastically depending upon the types of single crystals and polycrystalline piezoceramics like PZT.

1.6 Motivation for current work

To understand certain physical properties at low temperatures, below 4 K or so, we need to understand how the elastic, piezoelectric and dielectric coefficients of these materials change with temperature. Our main focus however is to look for the exact behavior of piezoelectric coefficient d_{15} of these single crystal and polycrystalline piezoelectric transducers with decreasing temperature. Two main aspects of motivation to current work are:

- i)* To understand the temperature dependence of piezoelectric moduli d_{ij} for PMN-PT, LiNbO₃ and PZT shear transducers.
- ii)* Find material with large d_{ij} or for large displacement actuator at temperatures ≤ 4 K.

The temperature dependence of the piezoelectric moduli could be explained with many aspects which become very important at low temperatures. The experiments being done in many experimental labs use these transducers for low temperature physical and mechanical properties measurements with some assumptions that their magnitude remains unaffected by the temperature changes below a certain temperature. Our interest lies specifically to better understand the mechanical properties of quantum crystals (at very low temperatures). This study would be very useful to understand the true values of parameters charac-

terizing the low temperature phases of the materials if we know the piezoelectric moduli of the crystals being used as actuators or sensors at low temperatures.

At low temperatures, below 20 mK, a large d_{15} value would be sensitive to small stress σ for measuring the elastic constants of the solid ^4He . The large strain value would be very useful to study to the plastic deformation of helium crystals. We would also like to choose a material for which the piezoelectric shear coefficient d_{15} is linear over different applied voltages. If the linear change in d_{15} with applied stresses is non-hysteric, the large plastic deformation of the solid helium crystals would be better understood. PMN-PT single crystals are very brittle at low temperatures and so far our experience shows that they will break below a certain temperature if epoxied to a surface. The reason could be the thermal contraction of the transducer or the epoxy. The change of domain walls geometry with temperature can also be a factor leading to an increased fragile behavior.

Considering all the selection factors after measuring the the low temperature d_{15} , we would be able to choose a particular transducer or a stack of transducers (actuator) with large deformation with negligible temperature dependence below say 2 K or so. For example Kawamata et al. developed a stack (actuator) of 36° Y-cut single crystal LiNbO_3 transducers . The stack was used to calculate the compressional piezoelectric coefficients d_{22} and d_{24} [5]. They fabricated 10 layers of transducers each with thickness of 0.5mm and with an area of $(10\text{mm})^2$. They stacked the layers with electrically conductive adhesive (Dotite FA-750A) and used brass as electrodes. They calculated the piezoelectric displacement to be 760 nm(± 380 nm) with applied voltage of ± 1 kV. Since the sensitivity was very high, they suggested the stack to be used in atomic force microscope (AFM) and STM applications. We plan to fabricate similar type of actuators specially for LiNbO_3 to get large piezoelectric displacements at low temperatures as it is evident from our results that the value of d_{15} doesn't change much with temperature for LiNbO_3 single crystals.

Our studies, however, would show in coming chapters that we cannot simply assume that the piezoelectric coefficients don't change with temperature below 4 K. The ultimate goal is to understand the elastic properties of single crystals of ^4He and ^3He at low temperatures. The coefficients d_{33} , d_{31} , and d_{15} need to be well defined to extract more reliable behavior of bulk and shear moduli of the single and polycrystalline helium crystals at low temperatures and high pressures.

Chapter 2

Literature review and background

2.1 Historical background-piezoelectricity

Pierre and Jacques Curie observed the surface charges of crystals, such as tourmaline, quartz, topaz, cane sugar and Rochelle salt upon application of pressures [6]. They observed the macroscopic polarization or accumulation of charges on surfaces of some materials named above and they published a paper showing these effects in 1880. The phenomena was named as piezoelectricity. The Greek word piezo means to press, meaning the production of electric current by applying the pressure. This unique name to this particular phenomena was helpful in distinguishing this mechanism from the the other research problems of that time, e.g contact electricity and pyroelectricity [7].

Later in 1881, Lippmann predicted mathematically that the converse of piezoelectric effect must also be true [6] and Curie verified this converse effect experimentally. By the start of World War I, many of the thermodynamic and physical properties of various piezoelectric materials were studied substantially. Robert William Boyle (October 2, 1883 to April 18, 1955) was a Canadian physicist and served as a head of department of physics and dean of science

at the University of Alberta (1912-1928) and was one the of most important early pioneers in the development of sonars, being considered as father of sonar technology. In late 1917, Boyle and a small team of British researchers studied the earlier work of French physicist Paul Langevin in acoustic underwater detection, and developed an ultrasonic quartz transducer that could be used as sound navigation and ranging (sonar). Their development became the first practical use of sonar in warfare. After the first successful application as sonars, many research groups all around the world started working on these materials and developed many applications like microphones, accelerometers, ultrasonic transducers, etc. on a commercial basis. During and after World War II, people started developing other synthetic materials such as piezoceramics which proved to be a big step ahead in this field as ceramics were more sensitive and it was quite easy to replace the old technology as well as increase the applications of the piezoceramics.

Both direct and converse piezoelectric effects are observed in single crystals and polycrystalline materials. We start with generalized tensor equations and later we will see how these equations evolve under specific crystal structure depending upon the symmetry considerations in crystals and in tensors. The generalized piezoelectric phenomena, for small strains and linear piezoelectric materials, can be described by the following equations [8].

$$D_i = \kappa_{ij}^\sigma E_j + d_{iu} \sigma_u \quad (2.1)$$

and

$$\epsilon_k = d_{jk} E_j + S_{ku}^E \sigma_u \quad (2.2)$$

where D_i is the electric displacement vector, κ_{ij} represents the dielectric permittivity at constant stress, σ_u is the stress vector, E_j is electric field vector, ϵ_k is the strain tensor and d_{iu} are the reduced indices piezoelectric coefficients. These equations vary differently depending upon whether we consider single

crystals or ceramic polycrystals. We will see the modified versions of these equations in following sections.

2.2 Paraelectricity, ferro-electricity, and piezo-electricity

If a partial electric charge appears at one side of an atom or molecule which induces equal amount of negative charge on the other side because of electrostatic attraction, then the distribution of positive and negative charges of equal magnitude and opposite polarity creates electric dipoles. The product of the magnitude of the charge and the separation between two charges is called electric dipole moment. These dipoles are vectors and, when added, give a net polarization to a ferroelectric material. The crystal symmetry dictates that the crystals having center of symmetry cannot have a net polarization so they cannot be piezoelectric. The ferroelectric crystal must be non-centrosymmetric in order to have a net polarization even in absence of all external factors. This suggests that the atoms at certain positions at lattice sites must go out of their equilibrium positions in order to get a net electric polarization and resulting ferroelectric behavior. Materials can be polarized by displacing the atoms along a particular axis giving a net dipole moment along that particular crystallographic direction.

When single crystals, e.g LiNbO_3 , are cooled below the Curie temperature T_c (1410 K), the paraelectric phase transforms into a ferroelectric phase in which the Li and Nb atoms move to new positions and induce spontaneous electric polarization. However there can be many domains in a newly-grown single crystal with local magnitudes and directions. The application of an external electric field switches the polarization to one particular direction and this net polarization is frozen by decreasing the temperature well below the ferroelectric phase transformation. Both LiNbO_3 and piezoelectric PMN-PT

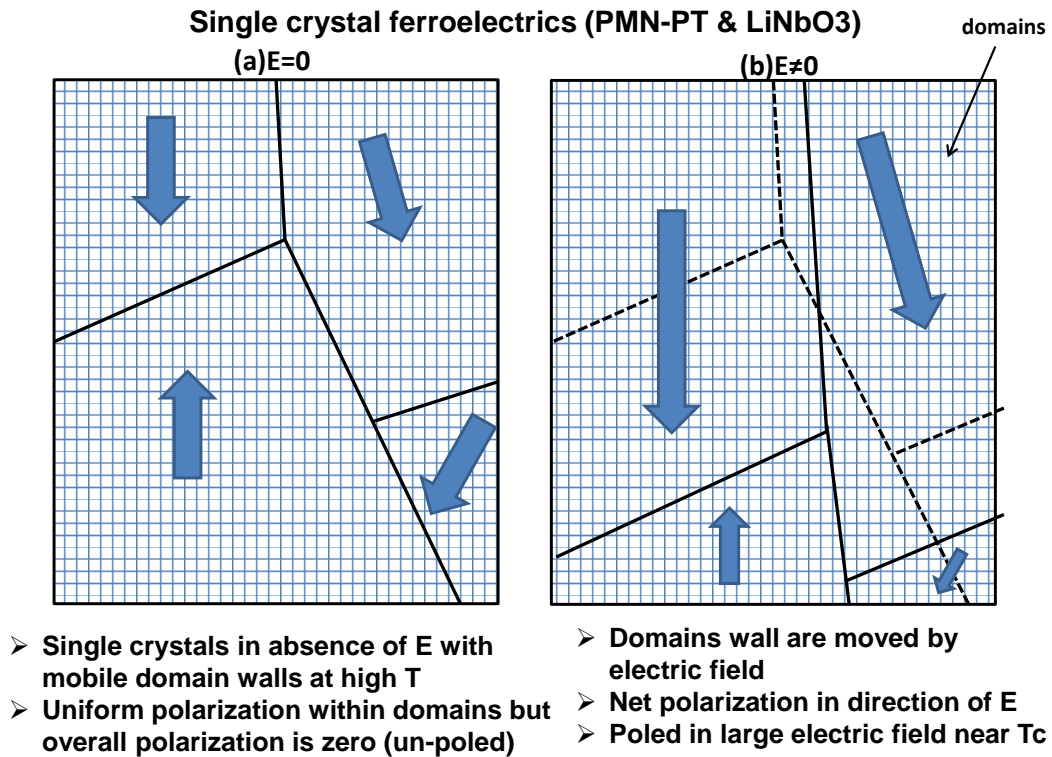


Figure 2.1: Unpoled (a) and poled (b) single crystals of LiNbO₃ and PMN-PT.

despite being single crystal, have random dipole orientations in different domains and there is no net polarization above and below the Curie temperature. They need to be polarized with a large electric field in a particular direction. Above the Curie temperature, single crystals of LiNbO₃ and PMN-PT are in paraelectric phase where they do not possess any polarization. Below the Curie temperature, the direction of the polarization could be anti-parallel in a domain relative to another domain connected to it via a movable domain wall. The boundary separating two such domains is called a 180° domain wall. The average value of electric polarization is zero. If a large electric field is applied, some domains get bigger as a result of motion of domain walls. There would be a net polarization in the single crystals in direction of electric field. The poling of crystals is usually done near the Curie temperature. The method is schematically explained in Fig. 2.1.

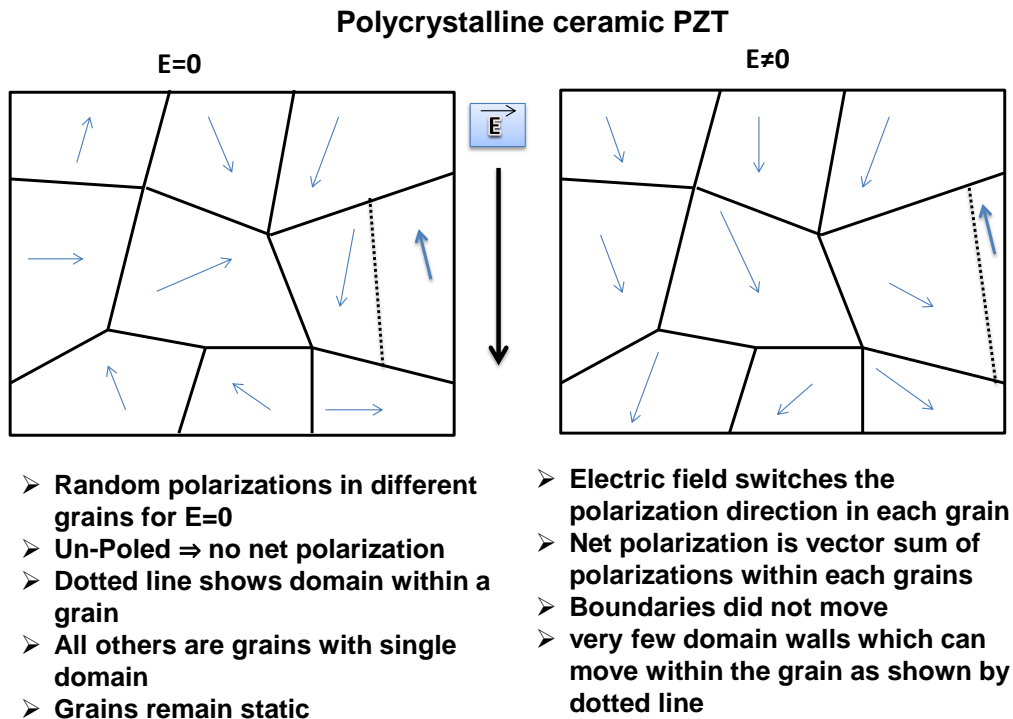


Figure 2.2: PZT crystals with random grains with different crystallographic orientations average polarization equal to zero. The grains did not move but the dipoles get oriented in direction of applied electric field during the polling process giving a net polarization to the crystal.

PZT is a polycrystalline material and PZT transducers must be poled below the Curie temperature in the ferroelectric phase. Different grains have different crystallographic orientations. The grain boundaries are fixed. The average value of polarization is zero. There could be very few domains within a grain but their number is small enough to be considered as negligible. When the external electric field is applied near the Curie temperature of PZT ($T_c=443-633$ K depending on the composition), the random polarization of individual grains is forced to align in the the direction of the field. The sample is cooled well below the Curie point in order to preserve the polarization as shown in Fig. 2.2.

A dielectric material can exhibit polarization in the presence of an external

electric field. It is non-conductor of electricity. All insulators exhibit electronic polarization to some extent and that's why they are dielectric to some extent. A permanent dipole is created in ferroelectric materials below the Curie temperature because of shifting of ions in the unit cell. The net concentration of positive and negative charges aligns towards opposite poles of a certain crystallographic directions giving rise to spontaneous polarization also known as ferroelectricity which is basic for any piezoelectric material. These polarized structures make local regions in the crystal and line up in a particular direction in a domain. This would give a net polarization to a single crystal. For polycrystals, however, there are randomly oriented crystallites with dipoles oriented in different directions and there would be no net polarization. We apply electric field so that these domains align with the applied field producing large polarizations. This polarization is directly related with the capacitance or ability to store electric charge. The capacitance of any material would then define the dielectric constant of that material which is a ratio between the capacitance of that material and the capacitance in free space.

2.3 Piezoelectric effect in single crystals

Single crystals of quartz, LiNbO_3 , and PMN-PT show a change in their electric dipole moment when a stress σ is applied. The strength of this electric polarization (dipole moment per unit volume) is proportional to the magnitude of the applied stress. Since single crystals are anisotropic, the state of the material is defined by a 9 component second rank stress tensor and a 3 component electric polarization vector. Let P_i be the polarization, which is related to the stress σ_{ij} by a 27 component piezoelectric modulus d_{ijk} . Hence the relation between polarization and the applied stress (in standard tensor notation) is

$$P_i = d_{ijk}\sigma_{jk} \tag{2.3}$$

where d_{ijk} is a third rank tensor and represents the piezoelectric moduli or piezoelectric strain coefficients. Here we associate 1, 2, 3 with X, Y, Z axes in the Cartesian coordinate system. Defining $i, j, k = 1, 2, 3$, we can write down an equation for the change in polarization vector in direction 1 upon application of stress.

$$\begin{aligned}
P_1 &= d_{111}\sigma_{11} + d_{112}\sigma_{12} + d_{113}\sigma_{13} \\
&+ d_{121}\sigma_{21} + d_{122}\sigma_{22} + d_{123}\sigma_{23} \\
&+ d_{131}\sigma_{31} + d_{132}\sigma_{32} + d_{133}\sigma_{33}
\end{aligned} \tag{2.4}$$

where $i = 1$, and $j, k = 1-3$. Similar equations can also be written for P_2 and P_3 . Now we consider an applied stress σ in direction 1 along the X-axis of a single crystal. The three polarization vectors in the crystal frame of reference along the z, x and y can be defined by $P_1 = d_{111}\sigma_{11}$, $P_2 = d_{211}\sigma_{11}$, $P_3 = d_{311}\sigma_{11}$. We can find out the values of d_{111} , d_{211} and d_{311} by measuring P_1 , P_2 and P_3 [9]. The stress tensor σ_{ij} is symmetric even in presence of body torques, i.e. $\sigma_{ij} = \sigma_{ji}$. Hence by considering the crystal symmetry, we may write

$$d_{ijk} = d_{ikj}. \tag{2.5}$$

Using the transformation law for a third rank tensor, a physical quantity M can be measured as a set of elements of a third rank tensor, i.e.

$$M_{ijk}' = c_{iu}c_{jv}c_{kw}M_{uvw} \tag{2.6}$$

where M_{ijk}' represents the physical quantity in the rotated (crystal) frame compared to its value given as M_{uvw} in the lab frame, c_{iu} , c_{jv} , and c_{kw} are the rotation matrices. By using the properties of the tensors, we can prove that d_{ijk} in equation 2.3 obey the transformation law shown in equation 2.6. Let's consider the crystal axes in lab frame O_{xi} which becomes O'_{xi} after the

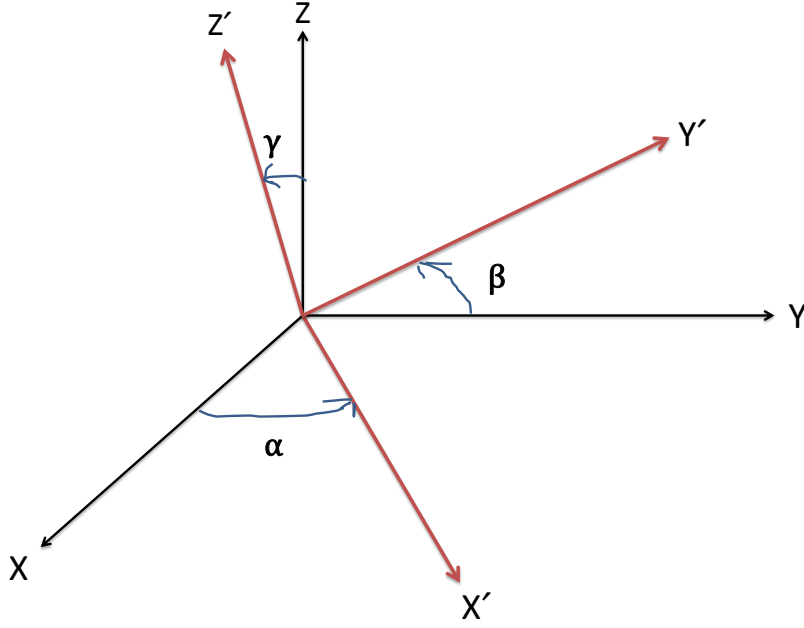


Figure 2.3: Transformation of axes to crystal frame from the lab frame.

transformation from unprimed to primed coordinate system. The components of the polarization vector in O'_{xi} frame are

$$P'_i = d_{ijk}' \sigma_{ij}' \quad (2.7)$$

as P'_i are related to P_i by a simple rotation of vectors i.e.

$$P'_i = c_{iu} P_u \quad (2.8)$$

and similarly the stress tensor σ'_{ij} can be related mathematically to σ_{ij} by a tensor transformation equation

$$\sigma_{ij} = c_{jv} c_{kw} \sigma'_{jk}. \quad (2.9)$$

Combining equations 2.9, 2.8 and 2.3, its easy to transform 2.7 as

$$P'_i = c_{iu} P_u = c_{iu} d_{uvw} \sigma_{vw} = c_{iu} d_{uvw} c_{jv} c_{kw} \sigma'_{jk} \quad (2.10)$$

Table 2.1: Symmetrical d_{ijk} leaves 18 independent components shown in brackets.

d_{1jk}	d_{2jk}	d_{3jk}
$\begin{bmatrix} d_{111} & d_{112} & d_{113} \\ d_{121} & d_{122} & d_{123} \\ d_{131} & d_{132} & d_{133} \end{bmatrix}$	$\begin{bmatrix} d_{211} & d_{212} & d_{213} \\ d_{221} & d_{222} & d_{223} \\ d_{231} & d_{232} & d_{233} \end{bmatrix}$	$\begin{bmatrix} d_{311} & d_{312} & d_{313} \\ d_{321} & d_{322} & d_{323} \\ d_{331} & d_{332} & d_{333} \end{bmatrix}$

and comparing 2.10 with 2.7, we might write

$$d_{ijk}' = c_{iu}d_{uvw}c_{jv}c_{kw}. \quad (2.11)$$

This equation is important merely because it shows how the transformed piezoelectric modulus d_{ijk}' is related to the untransformed/non-rotated d_{ijk} .

Now the value of the piezoelectric coefficient d_{ijk} matrix would be different depending on the crystal symmetries and their respective classes [10]. The general form of d_{ijk} is (for $i=1; j, k=(1-3)$) shown in table 2.1.

Now we will reduce the number of suffices in the above notation. Let's introduce a scheme (Voigt notation) where $[11, 22, 33, (23,32), (31,13), (12,21)]=[1, 2, 3, 4, 5, 6]$. We have now reduced the three indices of d_{ijk} to two and two indices of σ_{ij} to one. This scheme transforms equation 2.4 to

$$\begin{aligned} P_1 &= d_{11}\sigma_1 + \frac{1}{2}d_{16}\sigma_6 + \frac{1}{2}d_{15}\sigma_5 \\ &+ \frac{1}{2}d_{16}\sigma_6 + d_{12}\sigma_2 + \frac{1}{2}d_{14}\sigma_4 \\ &+ \frac{1}{2}d_{15}\sigma_5 + \frac{1}{2}d_{14}\sigma_4 + d_{13}\sigma_3 \end{aligned} \quad (2.12)$$

\Rightarrow

$$P_1 = d_{11}\sigma_1 + d_{16}\sigma_6 + d_{15}\sigma_5 + d_{12}\sigma_2 + d_{14}\sigma_4 + d_{13}\sigma_3 \quad (2.13)$$

where the factor $\frac{1}{2}$ is introduced just to avoid double counting and make the

calculations easier. Similar expressions can be written for P_2 and P_3 . In general,

$$P_i = d_{ij}\sigma_j. \quad (2.14)$$

The corresponding d_{ij} matrix is

$$\begin{pmatrix} d_{11} & d_{12} & d_{13} & d_{14} & d_{15} & d_{16} \\ d_{21} & d_{22} & d_{23} & d_{24} & d_{25} & d_{26} \\ d_{31} & d_{32} & d_{33} & d_{34} & d_{35} & d_{36} \end{pmatrix}.$$

Since the inverse of the piezoelectric effect is also true, when an electric field is applied to a piezoelectric crystal, it changes its shape. This behavior makes piezo crystals an excellent choice to be used as actuators. The relation between electric field E_i and the the produced strain ϵ_{ij} is linear and the piezo-electric coefficients d_{ijk} would remain the same as they were in case of direct piezoelectric effect

$$\epsilon_{jk} = d_{ijk}E_i. \quad (2.15)$$

Following similar steps as we did for direct piezoelectric effect, the reduced indices form for strains produced by the electric field is

$$\epsilon_j = d_{ij}E_i \quad (i = 1, 2, 3; j = 1, 2, 3, \dots, 6). \quad (2.16)$$

The strain tensor in single index notation would be

$$\begin{pmatrix} \epsilon_1 & \frac{1}{2}\epsilon_6 & \frac{1}{2}\epsilon_5 \\ \frac{1}{2}\epsilon_6 & \epsilon_2 & \frac{1}{2}\epsilon_4 \\ \frac{1}{2}\epsilon_5 & \frac{1}{2}\epsilon_4 & \epsilon_3 \end{pmatrix}.$$

Crystal symmetry plays an important role for piezoelectric behavior. A crystal with a center of symmetry is not piezoelectric. If we polarize a crys-

Table 2.2: 2-fold symmetry leaves 8 independent components of d_{ijk} shown in brackets.

d_{1jk}	d_{2jk}	d_{3jk}
$\begin{bmatrix} 0 & 0 & d_{113} \\ 0 & 0 & d_{123} \\ 0 & 0 & 0 \end{bmatrix}$	$\begin{bmatrix} 0 & 0 & d_{213} \\ 0 & 0 & d_{223} \\ 0 & 0 & 0 \end{bmatrix}$	$\begin{bmatrix} d_{311} & d_{312} & 0 \\ 0 & d_{322} & 0 \\ 0 & 0 & d_{333} \end{bmatrix}$

tal with center of symmetry by applying a uniform stress, the crystal will be unchanged when we invert, which means the polarization will change its direction and there is no net polarization left in the crystal. Analytically, a crystal possessing a center of symmetry can be described by the transformation matrix

$$c_{ij} = -\delta_{ij}. \quad (2.17)$$

Using the transformation law for piezoelectric coefficients

$$d_{ijk}' = c_{iu}d_{uvw}c_{jv}c_{kw} = -\delta_{iu}\delta_{jv}\delta_{lw}d_{uvw} = -d_{ijk} \quad (2.18)$$

with the center of symmetry argument and using the properties of the delta function, $d_{ijk} = 0$.

To illustrate more, we consider non-centrosymmetric crystals with a two fold rotational symmetry (diad) axis along direction 3. Then the transformation of all the axes would be $1 \rightarrow -1$, $2 \rightarrow -2$, $3 \rightarrow 3$. If we substitute this scheme in d_{ijk} , we find that everything is zero except for entries for which the sign of d_{ijk} doesn't change. So using equation 2.18, its evident that $d_{133} = 0$ and $d_{123} = d_{123}$ and so on giving table 2.2 illustrating that this change in the matrix under the transformation is different for different crystal structures/classes. We will now discuss how these coefficients change for single crystals LiNbO₃, single crystal PMN-PT and polycrystalline PZT.

2.3.1 Single crystal LiNbO₃

Laboratory made single crystal ferroelectric LiNbO₃ is mostly used for room temperature and high temperature electro-optical modulators and switches [11]. A standard Czochralski process is used to grow these crystals. A few of the hundreds of potential applications are oscillators in optics, actuators and waveguide circuits in optical fiber telecommunications. This compound is prominent among other candidates of ferroelectric oxides because of its outstanding piezoelectric properties. Bulk transducers are used in memory elements, acoustic delay lines, microwave tunable devices etc. Being a single crystal, its properties are anisotropic. Hence it is necessary to understand the mathematical formulation of representation (tensors) and their physical significance. Its crystal structure is either hexagonal or rhombohedral and is characterized by large pyroelectric, piezoelectric, electro-optic, and photo elastic coefficients. The simple crystal structure is given in Fig. 2.5. Below the Curie temperature (1210⁰C) oxygen atoms making ab-planes form the base of a distorted hexagonal structure. Above the Curie temperature everything is in a paraelectric phase where the Li atoms lie in an oxygen layer which is $\frac{c}{4}$ away from the Nb atoms which are centered between oxygen planes. The ferroelectric phase develops below the Curie temperature and the elastic forces within the crystal force the Li and Nb atoms to take new positions (thermodynamic equilibrium). This change in position of these two different charged species induce a spontaneous electric polarization. The displacement ferroelectric phase has following order of atoms along the c-axis, ...Nb, vacancy, Li, Nb, vacancy, Li,... [12]. The positions of the Li and Nb atoms are shown in Fig. 2.5 Lithium niobate crystals exhibit 3m point group symmetry [12], so the tensors which would describe the physical properties of this crystal must have at least 3m symmetry as the tensors cannot have less symmetry than the crystal itself as stated by Neumann's principle. The d_{ij} matrix for lithium niobate (in reduced subscript form) would be

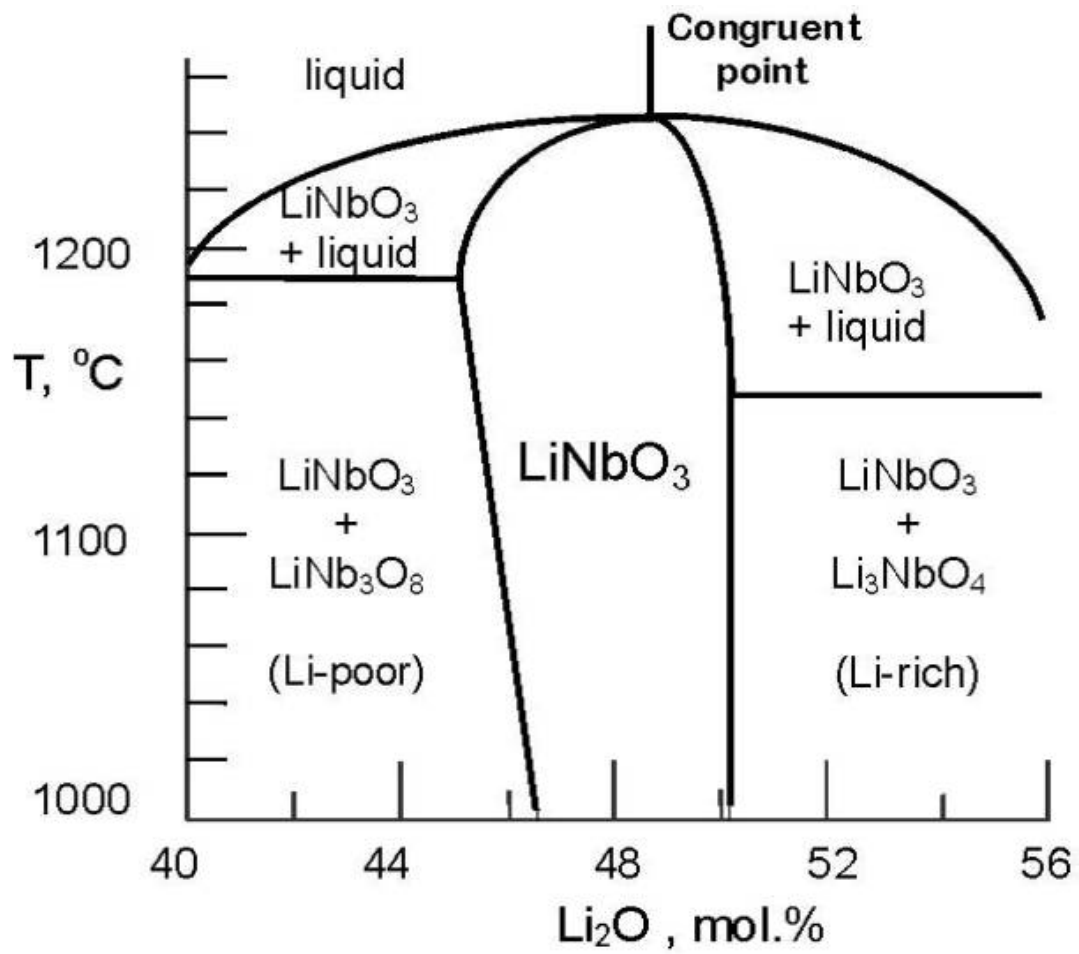


Figure 2.4: Single crystal LiNbO_3 : phase diagram for near LiNbO_3 with other well marked phases [13].

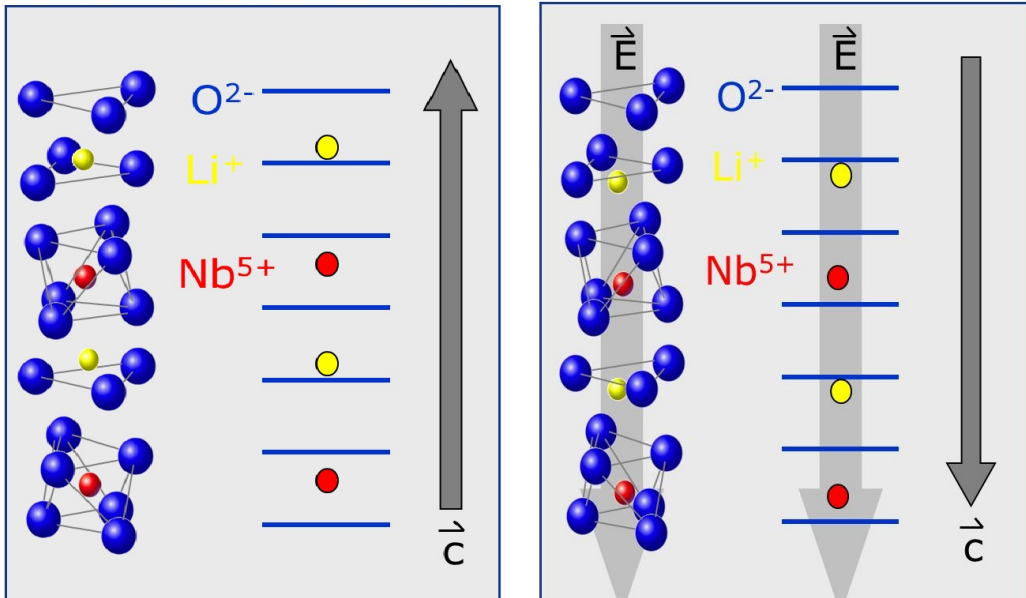


Figure 2.5: Single crystal LiNbO₃ : Nb⁵⁺ and Li⁺ ions on non-centrosymmetric lattice sites. The normal Li and Nb ions relative to the oxygen octahedral at room temperature are shown on left. Upon compression the ions move closer to their centered (paraelectric) positions with respect to the oxygen layers reducing the net polarization and leaving an excess amount of negative compensating charge on the + c face, causing the + c face to become negative. Transformation of paraelectric (left) to ferroelectric (right) phase [14].

$$\begin{pmatrix} 0 & 0 & 0 & 0 & d_{15} & -2d_{22} \\ -2d_{22} & d_{22} & 0 & d_{15} & 0 & 0 \\ d_{31} & d_{31} & d_{33} & 0 & 0 & 0 \end{pmatrix}$$

where the symmetry arguments give $d_{15} = d_{24}$, $d_{22} = -(\frac{d_{16}}{2})$ and $d_{31} = d_{32}$ [9]. Hence a LiNbO₃ single crystal can be fully described for its piezoelectric properties by four independent piezoelectric moduli i.e. d_{15} , d_{22} , d_{31} , d_{33} . For the inverse piezoelectric effect one can define the piezoelectric compliance tensor which would have S_{15} , S_{22} , S_{31} , S_{33} independent components using the same symmetry argument as we did for the direct effect.

Crystals are cut perpendicular to either X or Y direction (X -cut or Y -cut) depending upon what piezoelectric coefficients are required to be measured with the resulting transducers. The z -axis coincides with the symmetry axis according to the institute for radio Engineers (I.R.E) standards [15]. In Fig. 2.6, the X , Y and Z cuts are shown. The Z cut crystal is shown with a rotation just to have an idea of rotated crystal cuts. The detailed discription of X , Y and Z cuts for LiNbO₃ is given elsewhere [16].

The comparison of the temperature dependence of the elastic, piezoelectric, and dielectric constants for lithium niobate and lithium tantalate using the coefficients obtained from analytical solutions of ultrasonic wave mechanics was done in 1971 by R.T. Smith et al. [17]. The ratio of rate of change of elastic constant with temperature to the elastic constant for LiNbO₃ was varied as $-(2 \times 10^{-4})/^\circ\text{C}$ and the same ratio was measured for piezoelectric coefficients which was $(0.8 - 8.9 \times 10^{-4})/^\circ\text{C}$, where the dielectric permittivity tensor was found to be positive for single crystals of lithium niobate.

Warner et al. measured the elastic and piezoelectric constants for single crystals in (3m) class in general and lithium niobate and lithium tantalate as particular cases [18]. They used thin slabs of lithium niobate with gold plating (electrodes) on both faces and found a high effective coupling factor for lithium

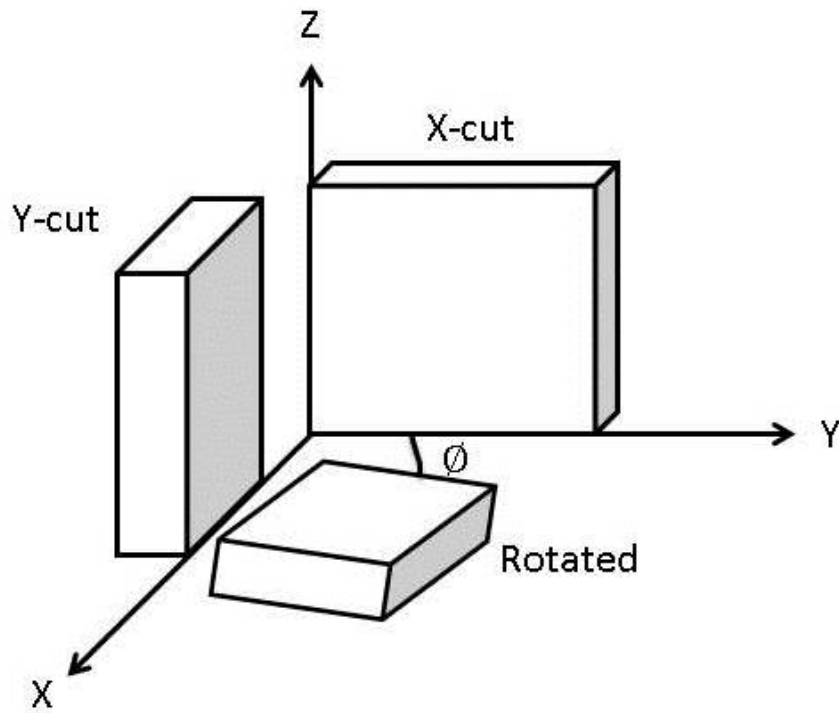


Figure 2.6: Crystal orientations and X, Y cuts with respect to z-axis. Single crystals of LiNbO_3 are cut after they are poled and annealed.

niobate and suggested it to be used in future transducer applications. The d_{15} value for lithium niobate was 6.8×10^{-11} m/V.

Another article came in the same era of late 60's when Tomoaki Yamada et al. measured the piezoelectric and elastic properties of single crystals of lithium niobate over a temperature range 20°C – 200°C [15]. They found the room temperature value of d_{15} as 74×10^{-12} m/V.

Hirotsugu Ogi et al. used the acoustic spectroscopy technique to determine the elastic, piezoelectric and dielectric coefficients of a bar shaped single crystal of lithium niobate [19]. They deposited a 100nm film of aluminum on the transducer surface (since lithium niobate is transparent and they needed it for reflections) and used a laser-Doppler interferometer with He-Ne laser beam. They observed 56 resonances over a frequency range of 0.3-1.2 MHz and determined the values for C_{ij} (elastic constants), e_{ij} (piezoelectric strain constants) with known values of k_{ij} (dielectric constant). The measured value of piezoelectric strain coefficient e_{15} was 3.65 ± 0.03 C/m² found to be consistent and more reliable than what the same group measured before. [19].

Kawamata et al. developed a stack (actuator) of 36° Y-cut single crystal LiNbO_3 transducers and calculated the piezoelectric displacement to be (760 ± 380) nm with an applied voltage of ± 1 kV. Since the displacement was very large compare to an individual transducer and the sensitivity was very high, they suggested the stack be used in AFM and STM applications [5].

2.3.2 Single Crystal PMN-PT

So far we have discussed single crystals of lithium niobate which exhibit intrinsic polarization and hence the associated piezoelectric character below the Curie point. Like LiNbO_3 , single crystals of PMN-PT have random dipoles and they need to be polarized by an external electric field. These are single crystals by structures but different ferroelectric domains have different orientations of dipoles and there is no net polarization until we pole them with

an external electric field. Ferroelectric PMN-PT can be fabricated as a single crystal or polycrystalline but observed single crystals properties are much better than polycrystalline ceramics. Single crystals of PMN-PT have very large piezoelectric coefficients which makes them an excellent choice to be used in many applications over a wide range of temperatures and frequencies, depending upon the size and shape of the transducers. Our main focus in this section is to understand the low temperature piezoelectric behavior of these transducers.

This compound was discovered by Smolenskii and Agronovskaya in 1958 and belongs to a special class of ferroelectric which is characterized by unusual piezoelectric, dielectric and elastic properties [20].

PMN-PT can be fabricated as a single crystal, polycrystalline ceramic or thin film, depending upon its potential applications. Their low Curie temperature $(130-170)^{\circ}$ C however, limits their applications in transducers used at higher temperatures. Single crystal PMN-PT exhibits the largest piezoelectric effect at room temperature which makes it the best actuator in all classes of ferroelectrics. PMN-PT single crystals are harder to produce but, once we grow them, we have a big advantage compared to PZT ceramics because of their large sensitivity and increased piezoelectric moduli. A problem with single crystals is that they are more fragile at low temperatures. We tested single crystal transducers epoxied to brass blocks at low temperatures and we found that every time we cooled down to temperature below the liquid helium temperature, they were broken. This might be due to anharmonic thermal expansion effect at low temperatures. The details of the comparison of PMN-PT with other ferroelectrics is given elsewhere [21].

The very first single crystal of $\text{Pb}(\text{Zn}_{1/3}\text{Nb}_{2/3})\text{O}_3\text{-PbTiO}_3$ or (PZN-PT) was grown by Nomura et al. using the flux method [22]. This was a start of growing single crystals having large and fast piezoelectric and dielectric response as compared to ceramic PZT. In 1990 Shrout et al. exchanged Zn with Mg and showed that the new compound $\text{Pb}(\text{Mg}_{1/3}\text{Nb}_{2/3})\text{O}_3\text{-PbTiO}_3$ or (PMN-PT) also

showed large piezoelectric and dielectric coefficients [23].

These crystals are prepared using the Bridgman technique in which a polycrystalline material is heated above its melting point and a seed crystal starts to form upon slow cooling from one end of the container in which the crystal is being grown. If the process is slow then a single crystal of the same crystallographic orientation as that of the seed crystal can be grown along the length of that container. This process is independent of the horizontal or vertical alignment of the container. These crystals are always grown near the morphotropic phase boundary (MPB) where the piezoelectric and dielectric properties are maximized. The MPB separates the rhombohedral and tetragonal phases of PMN-PT and PZT crystals on a composition vs. temperature phase diagram. Near the boundary, one gets high electromechanical coupling and large piezoelectric strain coefficients.

As an example, Yiping Guo et al. grew single crystals of PMN-PT near the morphotropic phase boundary. The single crystals of $(1-x) \text{Pb}(\text{Mg}_{1/3}\text{Nb}_{2/3})\text{O}_{3-x}\text{-PbTiO}_3$ directed in [110] direction were grown with different compositions ($0.30 < x < 0.35$) and subsequently poled under high electric fields ($2\text{-}30 \text{KVcm}^{-1}$). The crystal transformed from rhombohedral to monoclinic phase upon cooling near the MPB. This transformation was found to be irreversible as evident from the relation between temperature and the dielectric constant [24]. The phase diagram of the transition between two ferroelectric phases and a paraelectric phase is given in Fig. 2.7. The MPB separates the triclinic (T) and rhombohedral (R) phases. The cubic phase (C) is paraelectric and transforms to triclinic (T) upon cooling. Overall the irreversible phase transformation occurs in order R-Mc-T. We can see two-phase boundaries, i.e. rhombohedral-monoclinic and monoclinic-tetragonal boundaries, as shown in the unpoled PMN-PT phase diagram, linking the ‘O₁’ (PMN-30% PT) and ‘O₂’ (PMN-35% PT) composition regions. One can choose a particular composition within this region for optimum dielectric and piezoelectric properties.

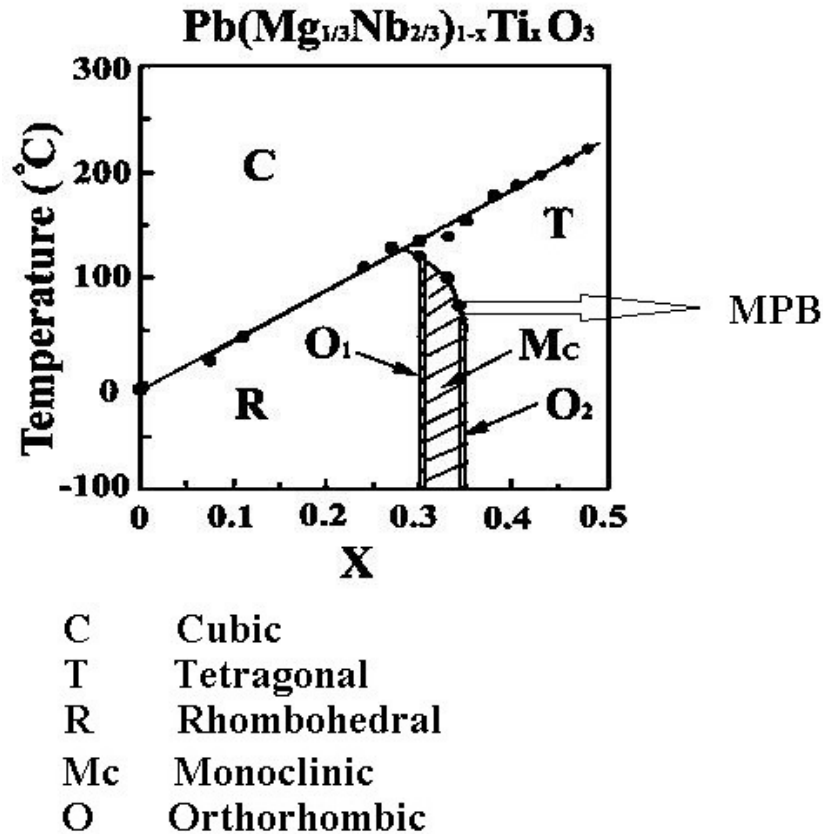


Figure 2.7: The phase diagram of PMN-PT showing tetragonal, rhombohedral and monoclinic phases. The region close to the MPB is the one where these crystals are known for maximum piezoelectric properties [24].

There are many aspects of the different properties of the piezoelectric transducers but we will focus on the variation of the piezoelectric coefficients from room temperature down to cryogenic temperatures. Jiang et al. studied PMN-PT actuators in 2005 over a temperature range (77-300 K) [25]. They designed actuators and piezo-motors with single crystals and tested their piezoelectric and dielectric behavior from room temperature down to liquid nitrogen temperature. However they only tested d_{33} and d_{32} for these transducers and one still needs to test for d_{31} and d_{15} , if they are to be used as piezo shear stacks at low temperatures.

Piezoelectric properties of ceramic PZT and PMN-PT were investigated in 2010 by Thiercelin et al. over a broad temperature range (10-300 K). Both the piezoelectric coefficient d_{31} and the dielectric coefficient κ_{33} were found to decrease at low temperatures for various chemical compositions of PMN-PT and PZT ceramics. Piezoelectric coefficients were found to change a lot with changes in chemical compositions. For example, the sample with PMN-42PT composition and tetragonal crystal structure showed the maximum value of d_{31} at 10 K [26]. Different compositions of PZT and PMN-PT showed different temperature dependences (not linear) in different temperature windows. The quality factor for all samples was found to initially increase with decreasing temperature (100-50 K) but then significantly decreased (lower than their room temperature values) below 20 K.

Feifei Wang et al. reported recent results of the temperature dependence of single crystals of PMN-PT. They measured piezoelectric moduli d_{33} , d_{15} , and d_{31} along with the elastic and dielectric coefficients from room temperature down to LN₂ temperature [27]. They grew the samples with the Bridgman technique, which were subsequently polarized and annealed for the optimum properties and the crystal structure was determined using X-ray diffraction. They used the resonant/antiresonant technique by using an impedance analyzer (Agilent 4294A) with a liquid nitrogen bath cryostat. Using the relations

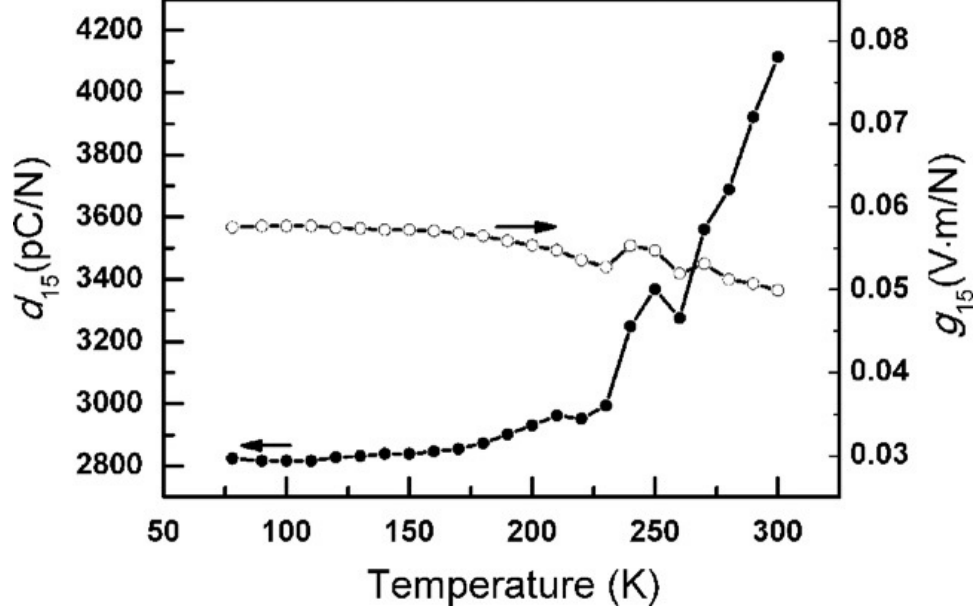


Figure 2.8: Temperature dependence of d_{15} and g_{15} : The decrease in d_{15} is quite prominent at higher temperatures and its very small at lower temperatures while the value for g_{15} increased a bit with decreasing temperature [27].

2.19, 2.20, 2.21, and 2.22, they determined the values of corresponding physical constants and plotted their behavior against temperature. The observed temperature dependence of d_{15} and g_{15} is given in Fig. 2.8. The experimental values of these constants decreased at low temperature (as expected) but the variations of piezoelectric, dielectric and elastic constants with temperature were different in different temperature regions.

Jiang et al. fabricated single crystal actuators of PMN-PT with different dimensions and polarization orientations [28]. Three of those samples are being discussed here. The first one was a stack in pure compressional mode with dimensions $10 \text{ mm} \times 10 \text{ mm} \times 50 \text{ mm}$, assembled by using $10 \text{ mm} \times 10 \text{ mm} \times 0.15 \text{ mm}$ single crystal plates of PMN-PT. The strain value at room temperature for an applied voltage of 150V was $65\text{-}85 \mu\text{m}$ and dropped to $30 \mu\text{m}$ at 77 K. The second actuator was designed by using the extensional transducers to measure the d_{31} coefficient. The actuator dimensions were $10 \text{ mm} \times 5 \text{ mm} \times 47 \text{ mm}$ which gave $\approx 285 \mu\text{m}$ deformation at room temperature reduced to about $100 \mu\text{m}$ at

liquid nitrogen temperature. The third sample was again fabricated for d_{31} coefficient with dimensions $10\text{ mm} \times 5\text{ mm} \times 7.6\text{ mm}$, showing a stroke of $50\text{ }\mu\text{m}$ at room temperature. The displacement of the actuator upon applying a voltage was measured using a linear variable differential transducer (LVDT) system for both room temperature and at LN_2 temperature. There was hysteresis in the voltage vs. displacement curves for all the samples. These actuators were intended to be used for space optics applications [28].

Another important study of lead-based ferroelectrics was carried out by Florian et al. in 2012. They grew single crystals in crystallographic directions using the so called Bridgman seed technique. These were poled and annealed to transform the paraelectric phase to the ferroelectric phase and freeze out the remnant polarization. They used the impedance method and determined the elastic compliance, dielectric constant, piezoelectric modulus and the related mechanical coupling factor and quality factor for different samples at different temperatures. Considering the importance of the MPB, they chose two samples (PMN-28PT) and (PMN-33PT) [29].

Piezoelectric, elastic and dielectric characteristics in both compressional and lateral modes were found to decrease with temperature with an interesting plateau region as compared to previous results. A relaxation mechanism was found at 100 K at the tail of the plateau region, which led to a considerable decrease in observed parameters. The coupling factor was found to be temperature independent above the relaxation (100 K). The observed high values and interpreted those arising from the presence of charges within the domain walls and phase instability affecting the polarization. The piezoelectric, elastic and dielectric coefficients for PMN-PT did not show a very rapid decrease until 100 K [29]. The temperature dependence of d_{31} and d_{33} , along with κ_{33} and κ_{31} is shown in Fig. 2.9.

The dielectric and piezoelectric properties of PMN-PT single crystals near the MPB were found to be strongly dependent on composition, poling field and

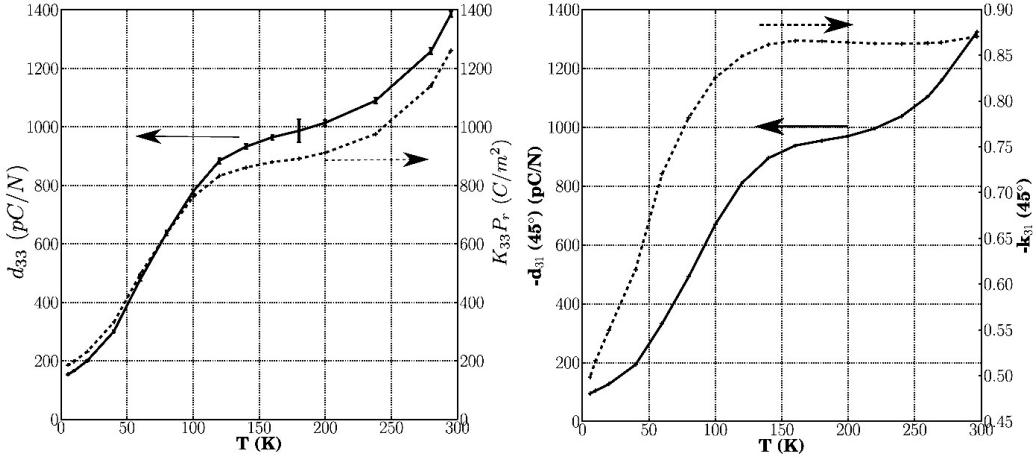


Figure 2.9: Temperature dependence of d_{33} , κ_{33} , d_{31} , and κ_{31} : The temperature effect before and after the relaxation mechanism along with the plateau region are quite prominent. One can see a sudden relaxation at 100 K [29].

polarization orientation [30]. PMN-PT single crystal plates were grown with PT compositions of 0.24, 0.30, 0.31, 0.33, 0.35 and 0.38, with corresponding poling fields 50, 250, 500, 750, 1000, 1500, 2000 and 3000 V. The samples were annealed in an oxygen atmosphere with temperatures of 131, 148, 156, and 164 °C for crystals grown in the (001) direction, at 129, 136, 149, and 161 °C for crystals grown in the (011) direction, and at 131, 149, 154, and 161 °C for crystals grown in the (111) direction. All the samples showed enhanced piezoelectric and dielectric coefficients $d_{33} > 1500$ pC/N and $\kappa_{33} > 0.92$. Similar work could also be done to understand the d_{15} and behavior of κ_{15} near the MPB. The properties of both single crystal and polycrystalline PZT and PMN-PT are strongly dependent on composition, annealing temperature, and crystal orientation [30].

We have extended the measurement of the piezoelectric behavior of single crystals of PMN-PT from room temperature down to 1 K for the pure shear mode d_{15} .

2.4 Polycrystalline PZT

Piezoelectric ceramics PZT or $\text{Pb}(\text{Ti}_x\text{Zr}_{1-x})\text{O}_3$ or $(\text{PbZr}_x\text{Ti}_{1-x})\text{O}_3$ are synthesized using the solid state reaction method and are being used widely for their piezoelectric properties. The Zr content determines the crystalline symmetry of this compound. Increasing Zr doping decreases the distortion in the tetragonal (4m) structure and eventually at $x > 0.52$, it transforms into a ferroelectric phase with rhombohedral (3m) symmetry. Compositions near the MPB are found to have the best piezoelectric properties. At the MPB, there are eight (111) directions for the rhombohedral phase and six for the tetragonal state in the (100) direction [31]. Phase changes at the MPB and the domain wall motions occur because of the poling process of the ceramic.

Ceramic piezoelectric materials belong to ∞m symmetry group which means they are described by three independent piezoelectric coefficients $d_{31} = d_{32}$, d_{33} , and $d_{15} = d_{24}$. Piezoelectric coefficients are strongly dependent on both external and internal factors. The materials must not be centrosymmetric in order to have piezoelectricity. The dipoles of the randomly oriented grains are polarized with an electric field in a particular direction, for example along the Z-axis or (001) direction. If we apply stresses parallel or perpendicular to the polarization, the values of the corresponding elastic moduli are different. If a tensile stress is applied perpendicular to the polarization direction, the polarization along Z-axis would reduce and if the stress is parallel to polarization, the Z-directed polarization would increase. These two phenomenon are d_{13} and d_{33} effects respectively [31].

Now if the shear stress is applied in such a way that the charges appear on the side faces, the piezoelectric coefficient measured is d_{15} which belongs to a pure shear mode of the transducer and is the objective of our current study. Schematic of the compressional, transverse, and shear modes of the piezoelectric ceramic transducers are given in Fig. 2.10. The magnitudes of the

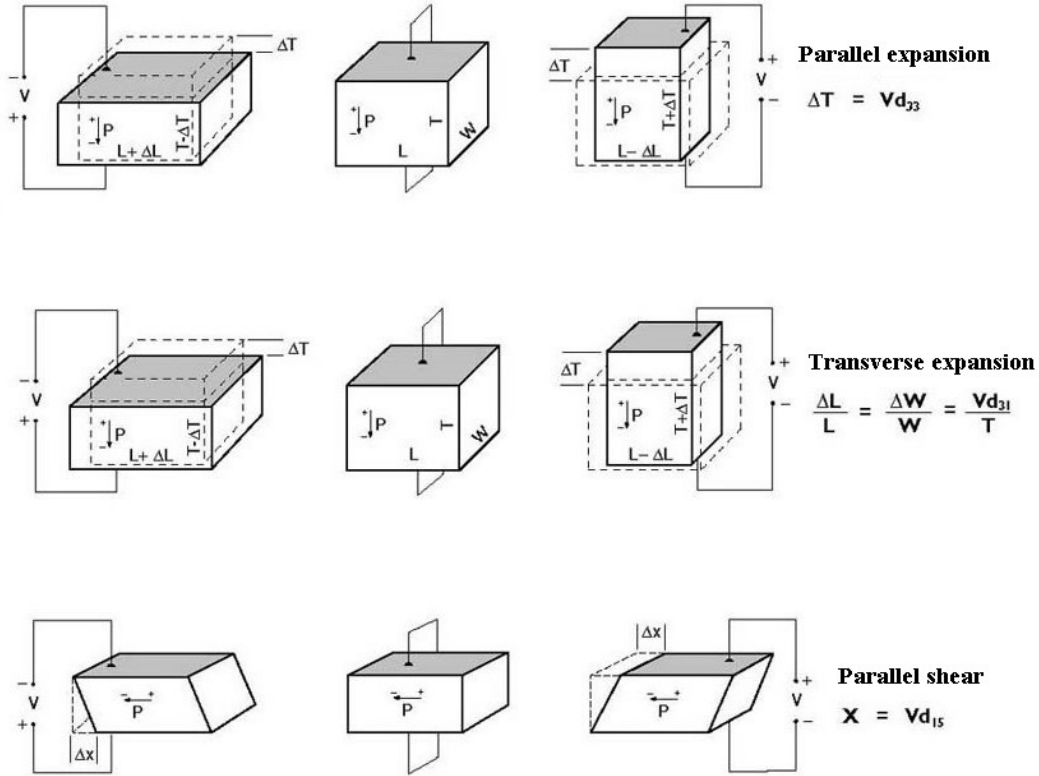


Figure 2.10: The three modes of operation of a piezoelectric transducer for which the polarization is directed along Z-direction. The compression, transverse and the shear modes of the transducers are related to the polarization direction [31].

piezoelectric moduli are influenced by the size of the piezo sensor/actuator. If we reduce the size of our transducer, we expect lower values of piezoelectric moduli as the number of grains and the grain boundaries in the sample and the piezoelectric properties are reduced and extrinsic contributions coming from the grain boundaries are decreased.

The MPB is a nearly vertical line between the tetragonal and the rhombohedral phase. The pure phases, divided by MPB, can be shifted by changing the compositions of the initial mixture. The transducers are designed and engineered by carefully selecting the composition on or near the phase boundary to maximize the piezoelectric properties [4]. This type of composition selection at MPB is under discussion in the scientific community and many point of views

exist for its explanation. For example Zhang et al. explained that piezoelectric and dielectric properties are enhanced by the large polarizability caused by the coupling between the tetragonal and rhombohedral phases. These two phases are equal energy states which allows an optimum fraction of domain reorientation during the poling process of the piezoelectrics [32]. The phase diagram of PZT is given in Fig. 2.11.

Doping with donor and acceptor impurities during the material preparation improves the overall piezoelectric characteristics of ceramic PZT. Soft PZTs like PZT-5 are obtained by doping with donors like ions Nb^{5+} or Ta^{5+} . Pb vacancies are created which can potentially ease the motion of domains resulting in soft crystals. If the precursor is doped with acceptors like Fe^{3+} or Sc^{3+} then the resulting final transducers will be harder because the oxygen vacancies pin the domain wall motion (specially at low temperatures) and the material gets hardened [33, 34].

The temperature dependence of d_{33} was measured for ceramics EC69 and EC70 (PZT commercial ceramic transducers) over a temperature range (300-4) K with Curie temperatures of 300°C and 200°C respectively. EC69 showed a moderate dependence on temperature i.e. the piezoelectric coefficient did not change much with temperature. The value at liquid helium temperature changed by only a factor of 2.2 compared to room temperature. For EC70 this drop was significantly larger and d_{33} dropped by a factor of 6. The temperature dependence of both of these samples is shown in Fig 2.15. This study used a technique to measure capacitance changes of parallel plate capacitors similar to the one we used in our studies [35].

K. Uchino discussed the issues regarding fabrication and performance of piezoelectric materials. There are some properties related to the material itself that can be altered by changing the chemical composition, polarization fields, annealing rates etc. to get the optimum properties [36]. His review concluded that the optimum doping in ceramic ferroelectrics is important to enhance the

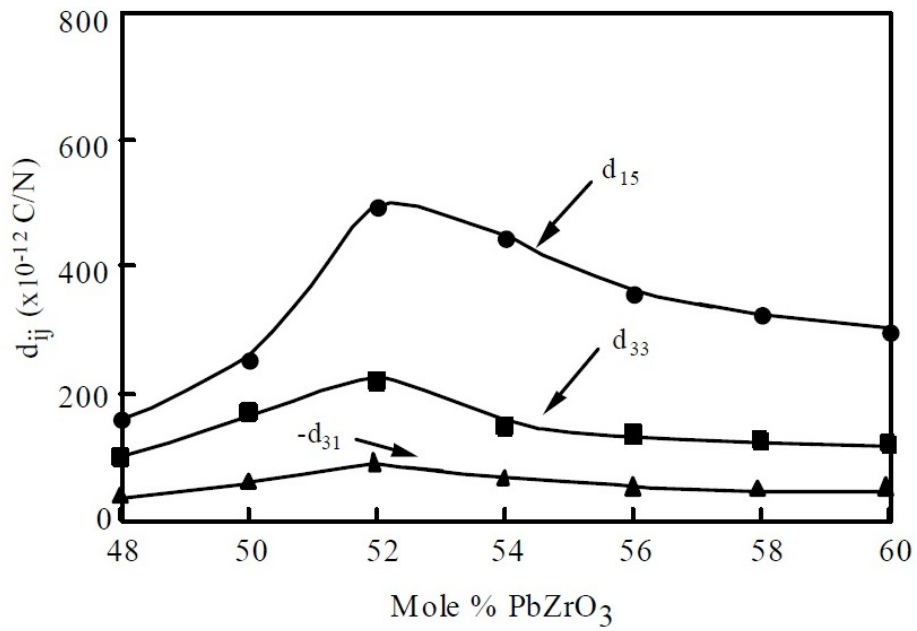
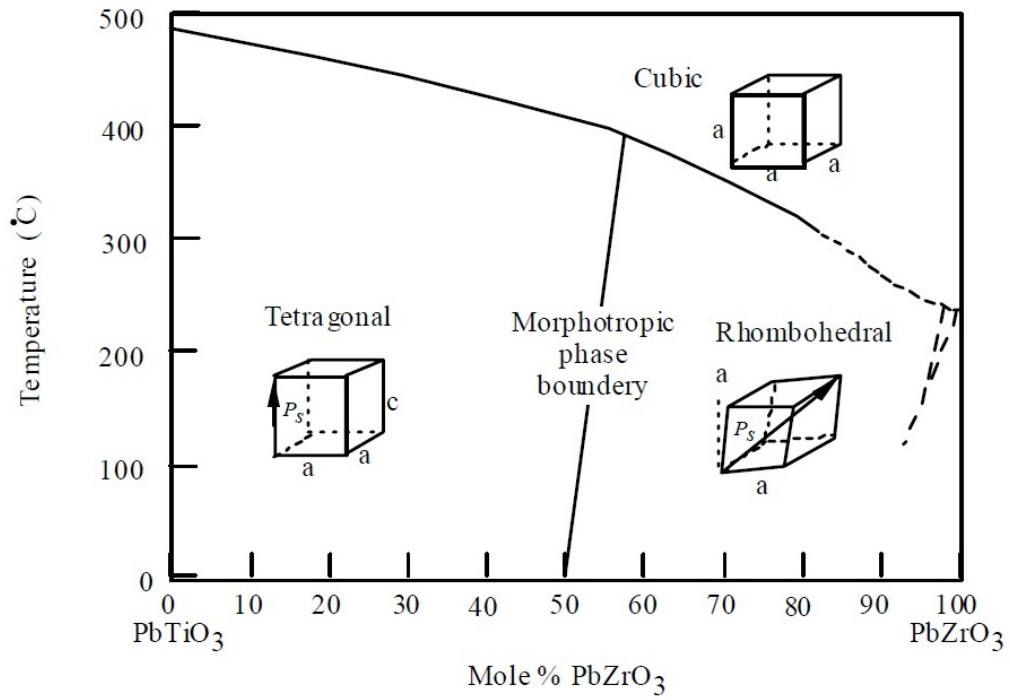


Figure 2.11: The phase diagram of PZT ceramics and the MPB separating the tetragonal and rhombohedral phases. Polycrystals grown on the MPB have the maximum piezoelectric properties (see the lower fig) [4].

strains and stabilize the temperature and external stress dependence [36].

Paik et al. investigated the piezoelectric and dielectric properties of perovskite ferroelectrics at low temperatures [37]. The piezoelectric properties were strongly dependent on the morphotropic phase boundary (MPB) compositions separating the tetragonal and rhombohedral phases. For example the soft and undoped PZT Navy type VI showed a decrease in d_{13} down to 50 pC/N below 100 K, compared to its room temperature value of 250 pC/N. The potential reasons for this behavior were the absence of external factors like domain wall motion and the shift in the MPB reducing the piezoelectric constants at low temperatures [38]. Another aspect of the study was to see how the compositionally adjusted Curie temperature of the ceramic changed affecting the piezoelectric coefficient near the MPB leading to engineering of the so called soft piezo ceramics [39]. The transducers were then fabricated using the altered compositions, i.e. doping La and Sn to get lower Curie temperatures to compensate for the loss of external contributions to piezoelectricity at lower temperatures. The compressional d_{33} was found to be increased to 250 pC/N at 30 K compared to its undoped value of 100 pC/N for PZTs. This increased value was associated with the re-adjustment of the composition in such a way that the resulting MPB at lower temperatures would lie on this composition.

PZT thin films were investigated for their piezoelectric and dielectric response, considering the fact that the composition plays an important role for low temperatures and lower dimensions. F.Xu et al. studied the piezoelectric response of PZT thin films with compositions near the MPB [40]. They figured out that both domain wall motion and extrinsic effects play a very important role in high temperature and bulk piezoelectricity. The values of the dielectric constants were found to be independent of film thickness (0.5-3.4 μm), polarization direction, and grain size for compositions near the MPB. This effect was probably due to 180° domain wall motion. The samples having thickness less than 0.5 μm showed a linear response to the applied electric potential. How-

ever when the film thickness changed i.e. ($1.5 \mu\text{m}$), samples showed a nonlinear response to the applied electric field. This was attributed to non- 180° domain wall motions. The effect turned on when the external excitations became more prominent i.e. in the thicker samples. They used non- 180° domain wall switching by applying the electric field over and under threshold magnitudes and concluded that the switching was almost zero for the thinner samples. The non- 180° switching was pinned for small thicknesses and became mobile at high thicknesses, increasing the probability of an increase in the room temperature piezoelectric coefficients [40]. The threshold switching field decreased with increased thickness suggesting an increased mobility of non- 180° domain walls. Matthew W. Hooker studied the piezoelectric, dielectric and ferroelectric properties of PZT-4, PZT-5H, PZT-5A and PLZT-9/65/35 type transducers over a temperature range of ($-150 - 250^\circ \text{C}$) in 1998 [41]. The piezoelectric constants d_{33} and d_{31} decreased by 50 percent for PZT-5A and PZT-5H compared to the room temperature values when temperature dropped down to -150°C . These coefficients were almost unaffected by temperature changes for PZT-4 while PZT-5A transducers possessed the highest value of piezoelectric coefficients at room temperature. The temperature dependence of these samples was roughly linear over the specified temperature window ($-150 - 250^\circ \text{C}$). PZT-5H transformed from its ferroelectric to its paraelectric phase above 170°C where its piezoelectric coefficients were the largest. The study suggested the very important role of choosing the appropriate materials for both high and low temperature applications [41]. The temperature dependence of both d_{33} and d_{31} is shown in Fig. 2.12.

2.5 Review of experimental methods

In this section we review the experimental techniques that have been used for measuring the piezoelectric moduli of piezoelectric transducers. This

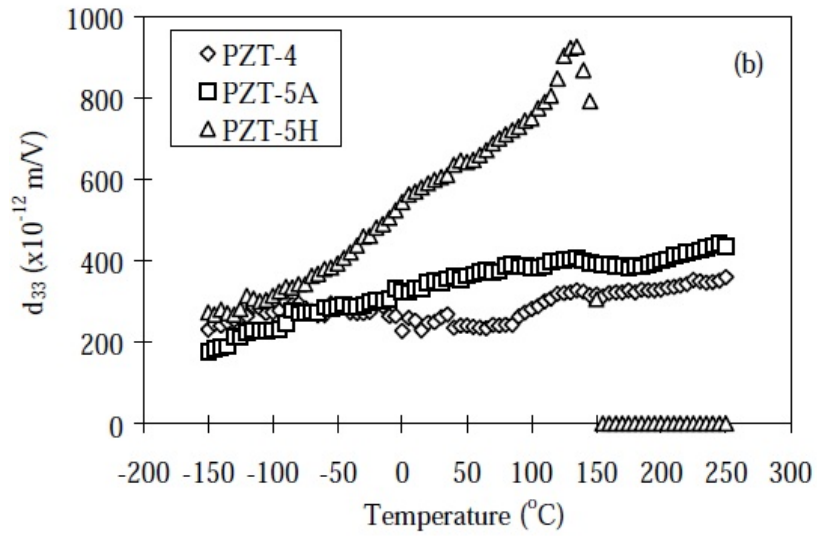
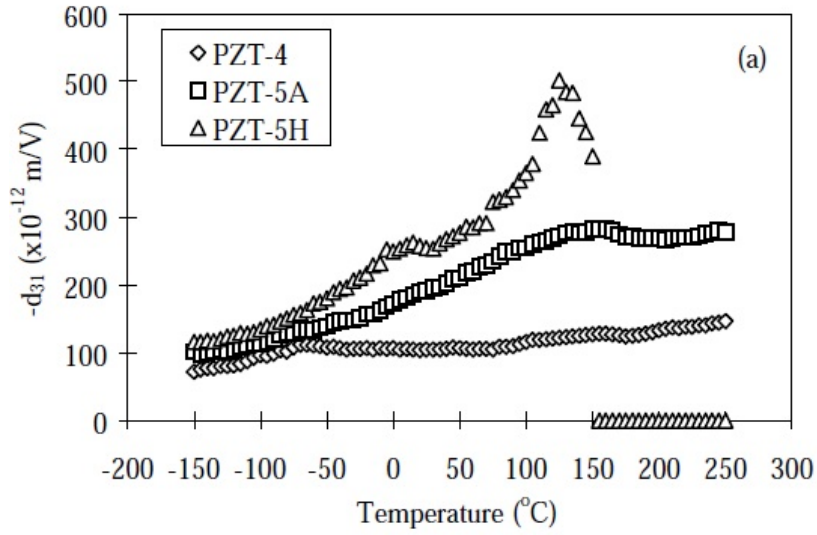


Figure 2.12: Typical temperature dependences of d_{33} and d_{31} for PZT-4, 5A, and 5H type transducers [41].

includes both resonance and direct displacement measurements.

The temperature dependences of the elastic, piezoelectric, and dielectric constants for lithium niobate and lithium tantalate were obtained from analytical solutions of the ultrasonic waves mechanics in 1971 by R.T. Smith et al. [17]. They studied electromechanical constants using ultrasonic phase velocity measurements combined with low frequency capacitance measurements, over a temperature window of (0 - 110⁰ C). They used the pulse superposition with phase comparison technique which had a resolution of 10⁻⁴. Two quartz transducers, each having frequency 45 MHz were used to measure sound speeds. Full details of the experimental set up and data acquisition are given elsewhere [17].

Warner et al. used the resonant/anti-resonant frequency method to measure the elastic and piezoelectric constants for single crystals in the (3m) class with lithium niobate and lithium tantalate as particular cases [18]. They used thin slabs of lithium niobate (thickness=0.2 - 1.00 mm) with gold plating (electrodes) on both faces having average surface areas of 0.25 cm². Piezoelectric transducers were excited in both compressional and the longitudinal modes. A frequency sweep method was used for higher overtones frequencies of the thin plates.

A schematic of the resonance/antiresonance method is given in Fig. 2.13. The single crystals were poled and then cut according to I.R.E standards. The orientations of the X , Y , and Z cuts were measured with X-ray diffraction. The surfaces were gold plated for electrodes and an AC signal was applied in the directions determined by the cuts and coordinate planes. The resonant and antiresonant frequencies were analyzed with the following equations. When the polarization direction is either in X or in Y directions, then the relation between the electromechanical coupling factor k_{31} , resonance frequency f_R and anti-resonance frequency f_A is given by

$$\frac{k_{31}^2}{1 - k_{31}^2} = -\pi \frac{f_A}{2f_R} \cot \pi \frac{f_A}{2f_R} \quad (2.19)$$

and the relation between the coupling factor k_{31} and elastic, piezoelectric and dielectric constants S_{11} , d_{31} and κ_{33} would be

$$k_{31}^2 = -4\pi \frac{d_{31}^2}{S_{11}^E \kappa_{33}^T} \quad (2.20)$$

and the resonance frequency of the transducer is

$$f_R = \frac{1}{2l\sqrt{\rho S_{11}^E}}. \quad (2.21)$$

The capacitance C across the plates at low frequencies is given by

$$C = \frac{\kappa_{33}^T wt}{4\pi l} \quad (2.22)$$

where $l \times w \times t$ are dimensions of the sample. A similar set of equations could be obtained for polarization in the z direction. Details of the full calculations are given in reference [15]. By measuring f_R , f_A , C and the set of different elastic and piezoelectric coefficients, they calculated a set of values for d_{15} and observed a small decrease in its amplitude with temperature, as shown in Fig. 2.14.

Hirotsugu Ogi et al. used an acoustic spectroscopy technique to determine the elastic, piezoelectric and dielectric coefficients of a bar shaped single crystal of lithium niobate [19]. The parallelepiped shape bar had dimensions of $L=5.039$ mm, $W=5.070$ mm and $H=4.973$ mm. They deposited a 100 nm film of aluminum on the transducer surface (since lithium niobate is transparent and they needed it for reflections) and used a laser-Doppler interferometer with a He-Ne laser beam. The laser was used to detect the displacement distribution on the vibrating surface of the transducer, which was excited with an input signal and another lead was used to detect the output.

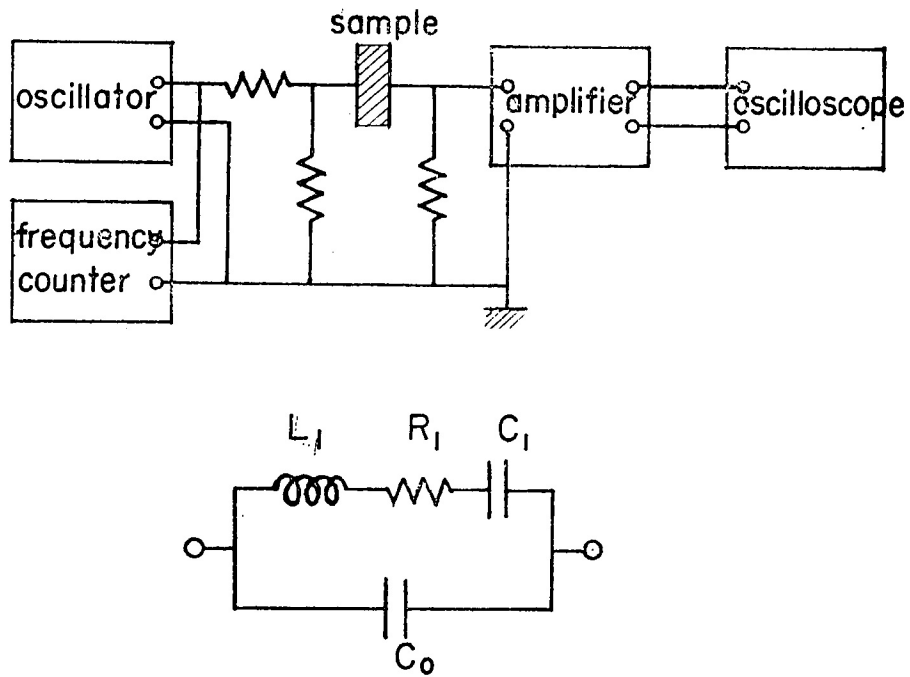


Figure 2.13: A piezoelectric vibrator circuit : the resonance/antiresonance set up for measuring elastic and piezoelectric constants of the single crystals of lithium niobate is analogous to the simple RLC circuit shown below the actual set up [15].

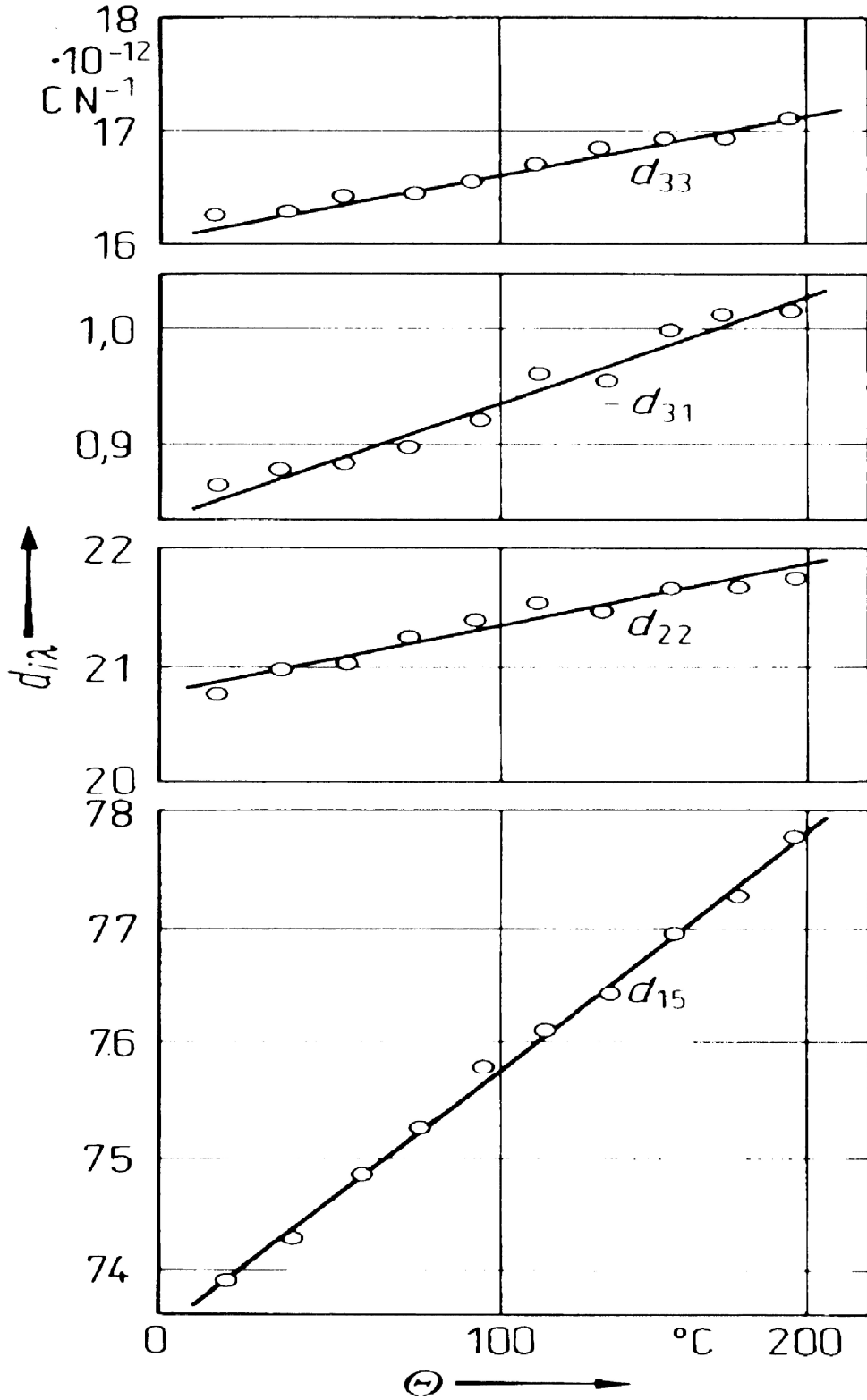


Figure 2.14: Temperature dependence of piezoelectric coefficients of LiNbO₃: comparison of the temperature dependence of the piezoelectric coefficients [15].

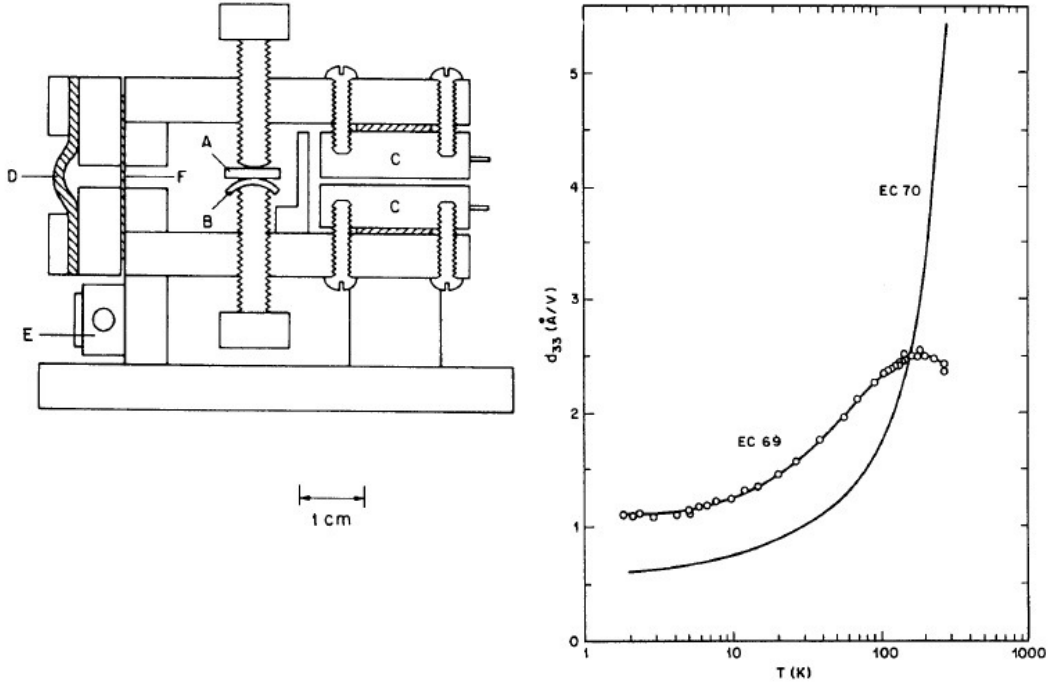


Figure 2.15: Piezoelectric displacement tester (left): when a voltage is applied across the actuator, the thickness of the actuator A changes, causing a capacitance change between two plates labeled as C, which is used to calculate the piezoelectric coefficient. The temperature dependence of d_{33} for two different samples. Ceramic EC 70 has a large temperature dependence with a lower d_{33} value at liquid helium temperature compared to EC 69 [35].

B. Yurke et al. designed and successfully tested a cryogenic piezoelectric displacement tester in 1986. They designed a lever-fulcrum device containing the lever arm with fulcrum at one end and the a capacitor at the other end. The PZT-5A ceramic transducer was mounted between the fulcrum and the capacitor. When a voltage was applied across the transducer, it produced a deformation in the material as consequence of inverse piezoelectric effect. This change in shape caused a change in the spacing between the capacitor plates. Knowing the dimensions of the capacitor plates and spacing between two plates, they were able to find the value of d_{33} by using the formula $d_{33} = \frac{\Delta l}{\Delta V}$ where Δl was a change in the dimensions of the transducer under an applied voltage ΔV [35]. The experimental set up along with the results obtained for two different

samples are given in Fig. 2.15.

Table 2.3: The table summarizes the piezoelectric coefficients measured so far using different experimental techniques. The values are quoted for different temperatures.

Temperature (K)	Piezoelectric modulus ($\times 10^{-12}$ m/V)	Reference
300	$d_{15} = 68$	LiNbO ₃ [18]
300	$d_{33} = 8$	LiNbO ₃ actuator [5]
30	$d_{33} = 393$	PZN-PT actuator [25]
30	$d_{31} = 315$	PZN-PT actuator [25]
300	$d_{33} = 140$	PMN-38PT [26]
100	$d_{33} = 122$	PMN-38PT [26]
20	$d_{33} = 32$	PMN-38PT [26]
78	$d_{31} = 831$	PMN-xPT [27]
78	$d_{15} = 2823$	PMN-xPT [27]
5	$d_{33} \approx 180$	PMN-28PT [29]
5	$d_{31} \approx 160$	PMN-33PT [29]
≤ 100	$d_{31} \leq 50$	PZT [37]
30	$d_{33} = 250$	PLZT [37]
4	$d_{33} = 120$	PZT-EC69 [35]
4	$d_{33} = 60$	PZT-EC70 [35]
213	$d_{31} = 120$	PZT-5H [41]

We found experimental values of three independent piezoelectric coefficients d_{33} , d_{13} , and d_{15} in our literature review measured using different experimental techniques. The idea was to highlight the important numbers. We can now compare these values with our results.

We have developed a similar technique to determine the piezoelectric displacements by measuring the capacitance change across two parallel plates using a high resolution capacitance bridge. The technique is direct and reliable and is designed to measure the shear deformations in order to measure the temperature dependence of d_{15} .

Chapter 3

Experimental Techniques

This chapter provides a detailed overview of the experimental set up we used to measure the low temperature piezoelectric coefficients. It also includes the design of the jig, cryogenics, vacuum and pressure measuring techniques, data acquisition and analysis.

3.1 Cryogenics and low temperature

We used a new Precision Cryogenics System dewar to hold the liquid nitrogen and liquid helium. To ensure good thermal insulation, we pumped out the space between inner and outer surfaces of the dewar down to a pressure of 4×10^{-6} Torr, using a turbo pumping station. We used an indium seal on the vacuum can, pumped the vacuum can down to 10^{-5} Torr and leak tested it. We used liquid nitrogen to attain 77 K and liquid helium for achieving 4 K. The first cooling cycle from room temperature down to 77 K was achieved with liquid nitrogen. We used a slow transfer of liquid into the cryostat and used the enthalpy of the cold gas to avoid large boil offs. We siphoned out the liquid nitrogen completely by pressurizing the dewar with helium gas and started subsequent cooling with cold helium vapors. We used a very slow transfer (only cold helium vapors) to effectively utilize the enthalpy of cold gas

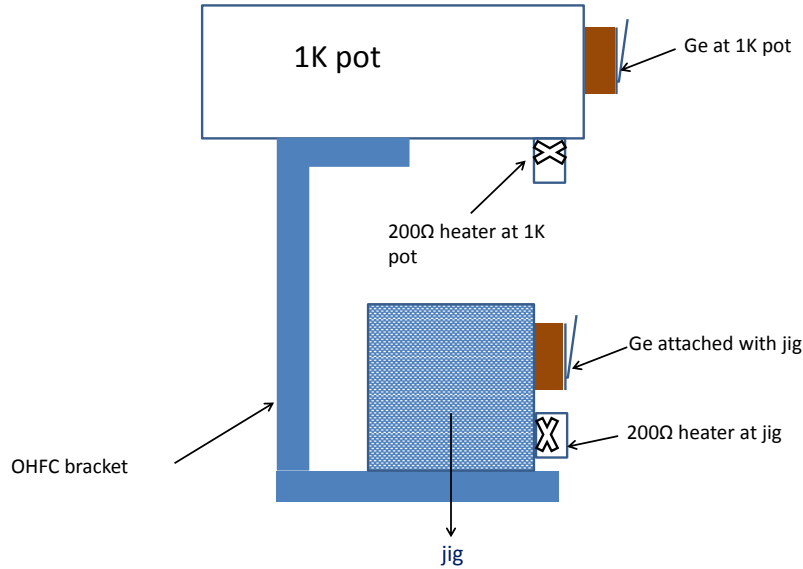


Figure 3.1: The oxygen free high conductivity copper (OHFC) bracket provides very good thermal contact between the pot and the experiment because of high thermal conductivity of copper even at lower temperatures. Thermometers and heaters on pot and jig are shown.

resulting in less boil off and expenses. We used few “shots” of helium exchange gas (10^{-2} Torr) for thermal contact between the experimental platform and the outside world of liquid helium. It took around 1 hour for everything inside and outside the vacuum can to reach down to 4K. Once everything was around 4 K, we increased the pressure in the liquifier/transport dewar up to 3 psi to transfer faster. The best transfer pressures for the liquifier and transport dewar for this new cryostat were 1.5 psi and 3 psi, respectively.

If we pump on a bath of liquid helium, we can attain 1.3 K or so, depending on the pumping speed and the size of the bath. This was achieved by pumping our 1 K pot. The vapor pressure of the helium in the 1 K pot drops exponentially with temperature and becomes very low for temperatures lower than 1.4 K. At this point there is very little cooling power. We refer to this as the 1 K pot cooling limit.

Our experiment was mounted on the 1 K pot via a bracket made with oxy-

gen free high conductivity copper (OFHC). This high purity copper provides excellent thermal contact between the pot and the experiment at low temperatures. The pot-bracket set up is shown in Fig. 3.1. The pot holds about a liter of liquid helium. We fill this pot every 24 hours for 5-10 minutes and then shut the siphon valve from the top of the cryostat and pump the pot with a mechanical pump. A vapor pressure of 450×10^{-3} Torr corresponds to the lowest stable temperature of the pot which is about to 1.25 K.

3.2 Thermometry

To measure the temperature of our experimental jig, we mounted a carbon glass thermometer CGR-1-2000 (C10607 by Lakeshore Cryotronics, inserted into a thermal anchor) on the jig. The thermometer was calibrated from room temperature down to 1.5 K. The other sensor was a Germanium GR-200A-2500-CD from Lakeshore Cryotronics calibrated from 1.4 K to 78 K, and it was mounted on a plate thermally anchored to the 1K pot. A schematic of the arrangement is given in Fig. 3.1. Two 200 Ω heaters are connected to the jig and the 1 K pot plate, respectively. The heater at the jig was mounted at a position lower than the temperature sensor, since the cooling starts up side down and heating (when applying power on heater) the other way. This scheme would help to achieve more stable temperatures with high sensitivity. The thermal relaxation time between the pot and the jig is small as they are thermally coupled by high purity copper. Oxford connectors, thermometers and temperature controllers are shown in Fig. 3.2.

3.3 Pressure measurements and leak-testing

A simple mechanical pump (dual stage) was used to pump the 1 K pot. The ultimate vacuum for this pump is of the order of 10^{-3} Torr. The pump is

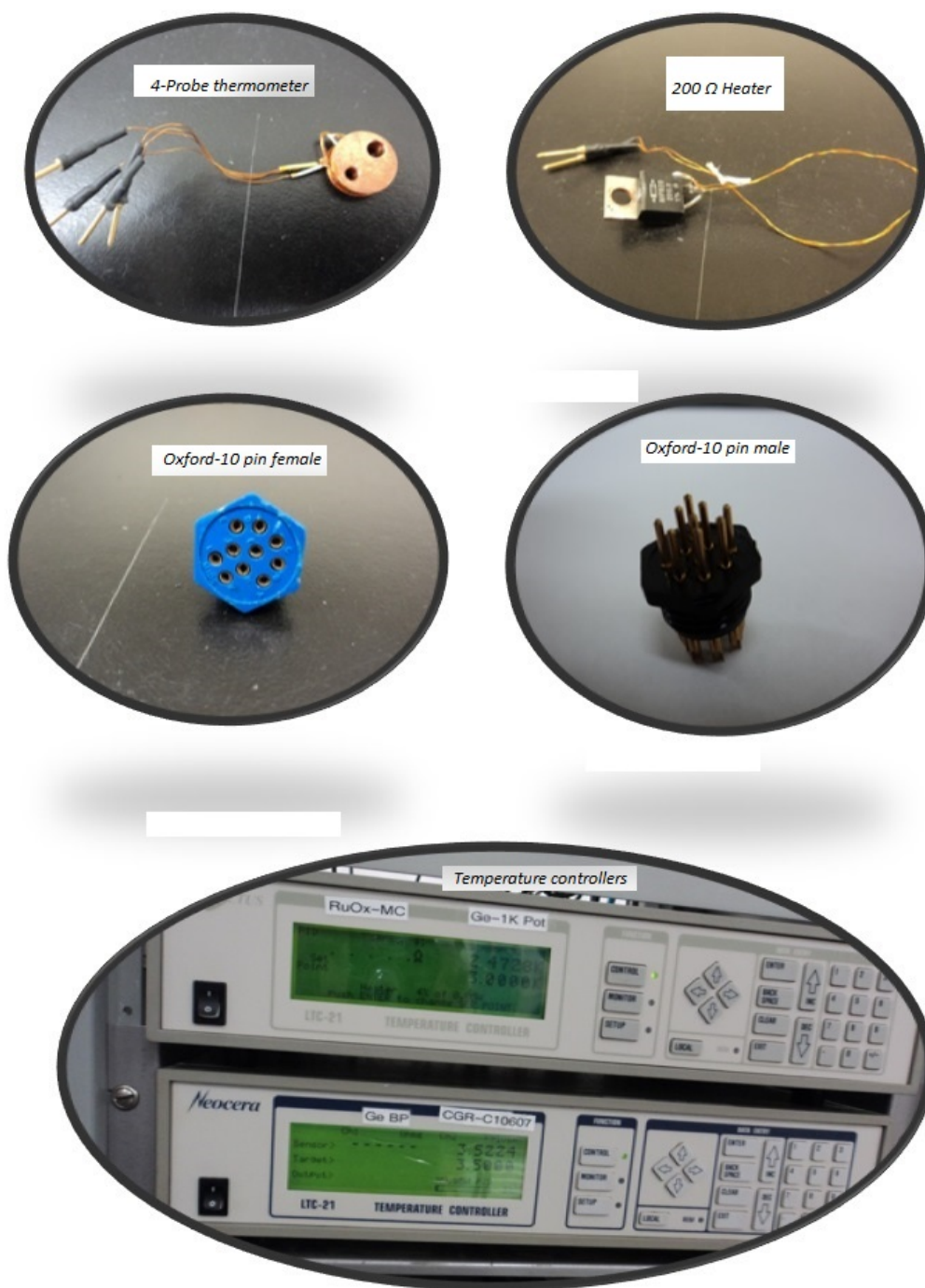


Figure 3.2: Ge and carbon glass thermometers, and heaters are connected to 10 pin female connectors on the 1 K pot plate. Cables from the male connectors on top of the cryostat couple with female connectors of the temperature controllers.

connected to the 1 K pot via flexible hoses, with a manual valve between the pump and the pot. We mounted a pirani gauge to measure the pressure between the manual valve and the pot. A turbo pump (Agilent technologies with V 81-AG rack controller) backed by a DS-102 Agilent roughing pump was used to pump out the vacuum can. This combination can attain the pressures as low as 10^{-6} Torr. A small tank of helium exchange gas is connected to the vacuum can via two manual valves. A few shots of this gas are enough to make thermal contact between the walls of the vacuum can and the experimental set up. For temperatures below 4 K and for leak testing the vacuum can top flange, we pump out the exchange gas for different times, depending on the temperature of the inside gas. Pirani and thermocouple gauges are used for rough vacuum measurements and a hot cathode ionization gauge is used for pressures below 10^{-3} Torr.

One of the most important things for low temperature measurements is leak testing. We used an ASM-110 Alcatel leak detector for leak testing of dilution refrigerators, flanges, vacuum can, different valves, the liquifiers, siphon and pretty much everything which we need to leak test for our experiments. Usually we leak check at room temperature, liquid nitrogen temperature and liquid helium temperatures. A leak detector is a combination of mass spectrometer, high vacuum chamber, pumps and vacuum gauges. The mass spectrometer can be tuned both for ^3He or ^4He , which helped us to use the leak detector to determine the ratio of ^3He to ^4He , of the mixture being used for dilution fridge operation.

3.4 Experimental design for measuring d_{15}

Detailed descriptions of the methods being used for measuring elastic, piezoelectric, and dielectric moduli were given chapter 2. The most important thing in this section is our design of the experimental set up for measuring the piezo-

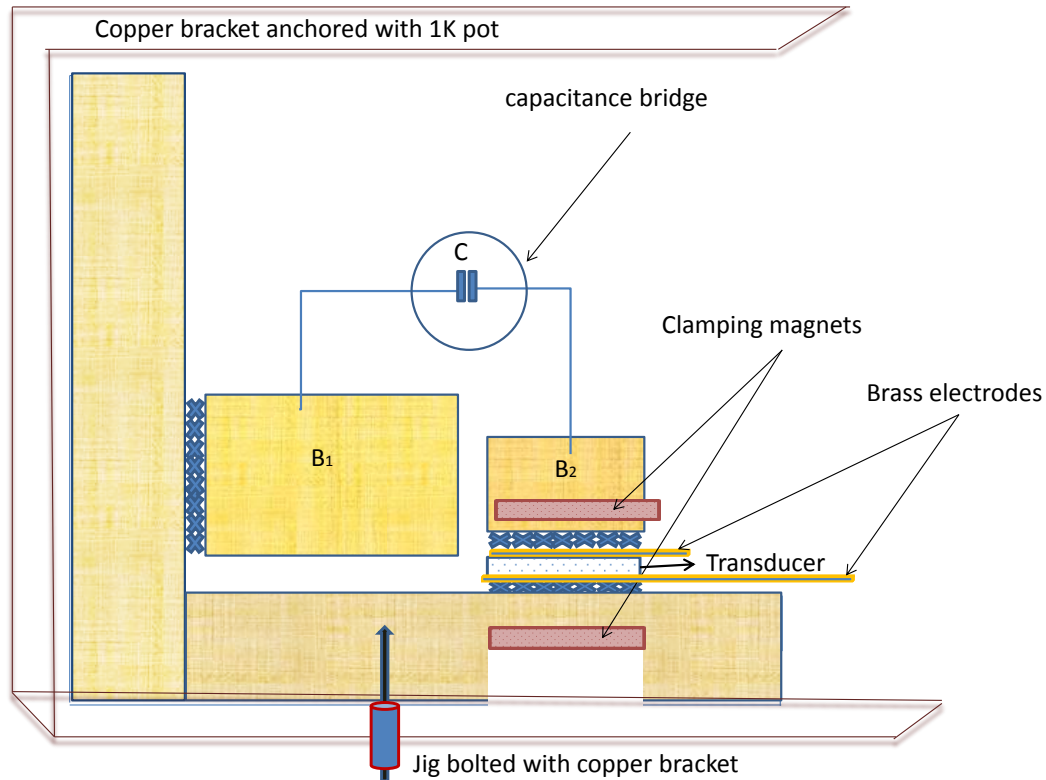


Figure 3.3: One out of three legs of the brass jig is shown here. The jig is sitting on the high purity copper bracket and bolted with the bracket in order to minimize the boundary resistance. Transducer, capacitance blocks (B1 and B2), electrically insulated epoxy, brass electrodes, clamping magnets, and the capacitance measurement scheme are shown in the schematic diagram.

electric coefficient d_{15} for PZT, PMN-PT and LiNbO_3 transducers. Initially we designed a brass jig with three legs in order to measure the piezoelectric coefficients for all three transducers with a single run of our cryostat. The idea was to save time and liquid helium but it didn't work because we had a common voltage connection for all three terminals and somehow the capacitance measurement of one set was affected by the voltage applied to the other two transducers at the same time. Hence we decided to take two measurements at a time with separate terminals for voltages. There are a total of 8 BNC coaxial cables connecting the 1 K pot plate with the top of the cryostat. We used two of those for applying voltage to the transducers and four for measuring the

capacitance changes across the plates. We have four Oxford 10 pin connectors connected with the 1 K pot plate. One can connect two thermometers and a heater with one 10 pin connector. These connectors are labeled as A, B, C, and D. We used all those connectors for 8 thermometers and four heaters. We checked the continuity of each on top of the cryostat and at the rear panels of the controllers, and capacitance bridges. We finally checked thermometers with the controllers by uploading the proper calibration files for the specific sensors. Brass is a very popular in the low temperature community because of its easy machining and non-magnetic nature at low temperatures. We designed and machined 3-legs brass jig for our d_{15} measurements. The experimental design of one of the three legs is shown schematically in Fig. 3.3. We prepared different connectors and thermal anchors and tested the jig on a bench by using the glass slides. Photos of the copper bracket, anchors and connectors, measurements on the bench, etc. are shown in Fig. 3.4

3.4.1 Mathematical formalism and measurements

When we apply a voltage ΔV across a shear transducer, it induces a transverse displacement Δx as a consequence of inverse piezoelectric effect. This produces a change in spacing ΔL between the two parallel plate capacitors of the jig as shown in Fig. 3.5. For linear piezoelectric materials and small changes, the strains in transducer can be approximated to be the same as the change in spacing between two capacitors plates ΔL .

$$\frac{\Delta L}{L} = -\frac{\Delta C}{C}. \quad (3.1)$$

The capacitance of a parallel plate capacitor is given by

$$C = \frac{A\epsilon_0}{L}. \quad (3.2)$$

Now consider a shear transducer with d_{15} as a shear coefficient. The change

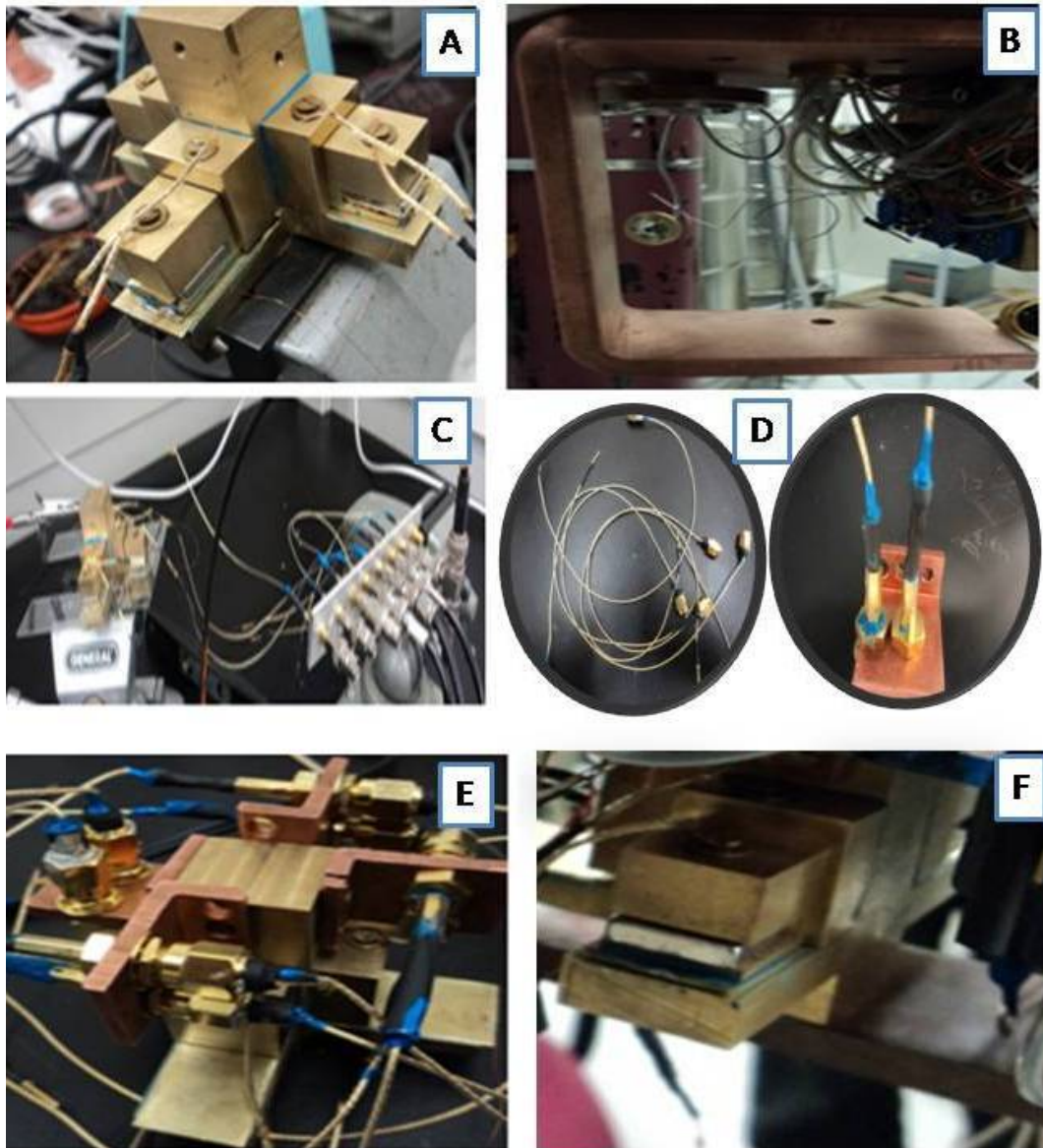


Figure 3.4: This figure depicts the step wise construction of the jig for measurement of d_{15} over a wide range of temperatures and voltages. Section A shows two blocks, capacitance and voltage leads, clamping magnets and epoxied plates. Section B of the figure represents the OFHC bracket attached with 1 K pot of the fridge. Section C shows the connectors and thermal anchors, Section D shows the test on the bench without thermal anchors and connectors on the jig, section E shows how we connected all the connectors with the thermal anchors on the jig to avoid the temperature gradients and section F shows the final view of the jig attached with the bracket to the 1 K pot.

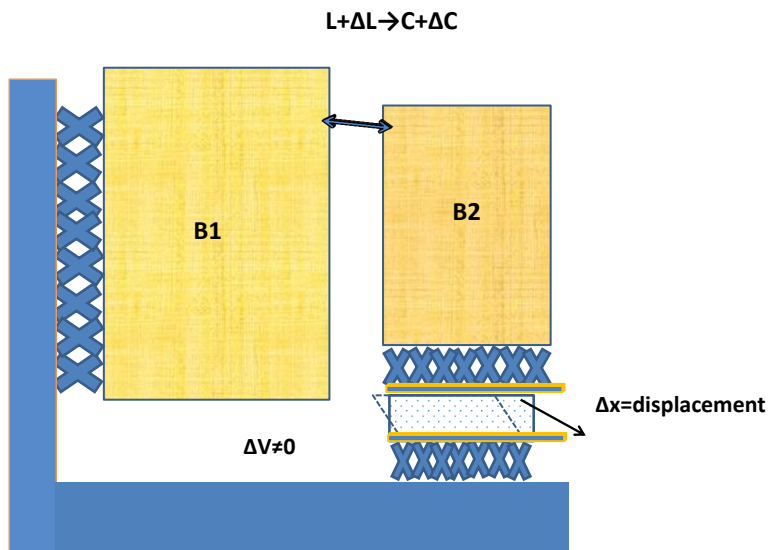


Figure 3.5: The change in capacitance for a parallel plate capacitor caused by the converse piezoelectric effect on the transducers can be accurately measured with a high precision capacitance bridge if the area of plates, and distance between plates is known.

in applied voltage across two faces of the transducer is related to the strain produced in the transducer by piezoelectric coefficient d_{15} . The schematic of measurement of capacitance for different values of input voltages on the transducers is given in Fig. 3.6. For a shear transducer,

$$\Delta x = d_{15}\Delta V. \quad (3.3)$$

The displacement of transducer moves block B2 and changes blocks separation i.e $L \rightarrow L + \Delta L$ i.e.

$$\Delta x = \Delta L. \quad (3.4)$$

The initial value of capacitance with $\Delta V = 0$, is given by

$$C_0 = \frac{A\epsilon_0}{L}. \quad (3.5)$$

When we apply a voltage, the shear displacement of transducer will move block B2 and the final value of capacitance across two blocks will be

$$C = C_0 + \Delta C = \frac{A\epsilon_0}{L + \Delta L} \quad (3.6)$$

$$\Rightarrow \Delta L = \frac{A\epsilon_0}{C_0 + \Delta C} - \frac{A\epsilon_0}{C_0} \quad (3.7)$$

for $\frac{\Delta L}{L} \ll 1$

$$\Delta L \simeq -\frac{A\epsilon_0\Delta C}{C_0^2} \quad (3.8)$$

since $d_{15} = \frac{\Delta x}{\Delta V}$, the final value of d_{15} is given as

$$d_{15} = -\frac{A\epsilon_0}{C_0^2} \cdot \frac{\Delta C}{\Delta V}. \quad (3.9)$$

We machined two bigger and two smaller blocks of brass and polished their faces as fine as with 3 micron polishing sheets. The surfaces of the main jig were

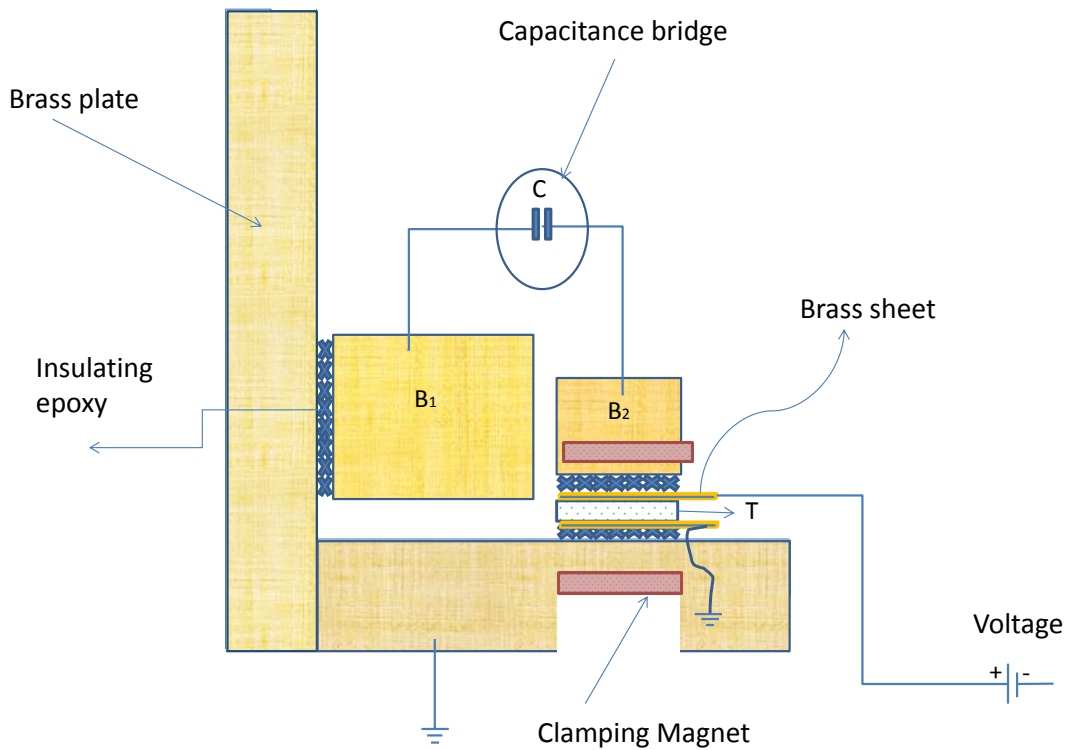


Figure 3.6: The schematic of capacitance measurements. Two brass blocks B1 and B2 are electrically isolated from the ground using the insulating epoxy. The shear transducer is clamped with two magnets. Two thin sheets of brass are used as electrodes. One face of the transducer is grounded and the other is used for applying voltage. We machined a square hole into the brass plate for lower transducer to get strong clamping and attach a support at the bottom so that it will not drop down when we remove the upper magnet.

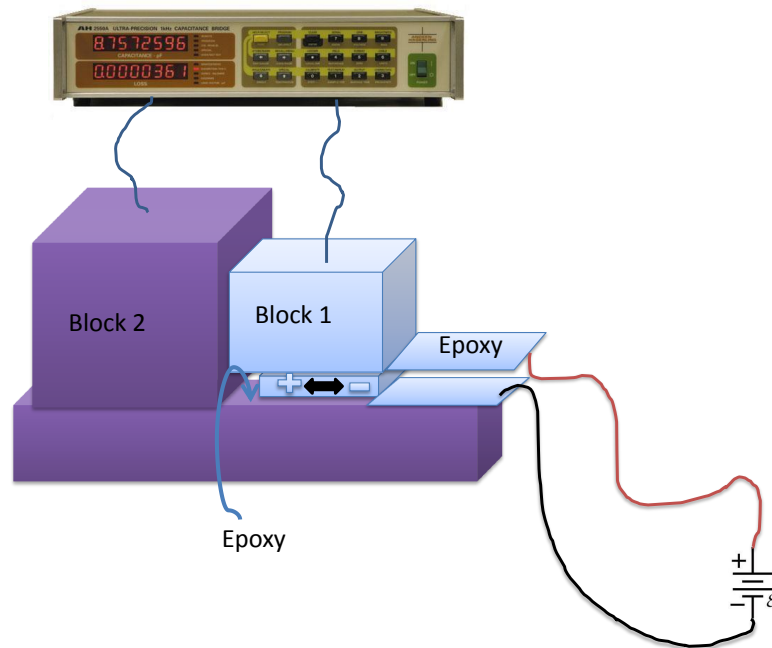


Figure 3.7: A 3-D view of jig: The shear displacement is related to the applied voltage by piezoelectric coefficient d_{15} for this particular polarization and applied stress on the transducer.

polished in similar way. We cleaned everything with dilute nitric acid followed by cleaning with water and methanol. The polished blocks were then epoxied using Hysol TRA-BOND 2151(3g), BIPAX epoxy for electrical insulation. Low thermal conductivity insulated wires were used to make the connections at low temperatures. We used a DC voltage source Keithley 2400 to apply variable DC voltage across the electrodes of the transducer. The capacitance between the blocks was measured with an AH 2550A ultra-precision 1KHz capacitance bridge. We averaged the capacitance measurements corresponding to each applied voltage for 9 seconds. This averaging time could be changed depending on the noise level in the data. A Labview VI was used to control the DC voltage source and to save the average values of capacitance to a data file. Sigma Plot 12.0 was used to analyze the data.

AH 2500A1 kHz automatic capacitance bridge offers great accuracy and resolution for capacitance and capacitance loss measurements. The resolution of 0.5 attofarad (0.000 0005pF) makes it a very sensitive capacitance measuring bridge. It can measure the dissipation factor as low as $1.8 \times 10^{-8} \tan \theta$. It can measure the capacitance in less than 0.5 second with full precision and make repeated measurements on the same sample in less than 40 milliseconds.

We know values for the effective area of the plates A , the average capacitance C and the change in capacitance and voltage ΔC and ΔV respectively. The two blocks were aligned using two glass cover slides as a spacer, with a separation between the blocks $L \approx 300 \mu\text{m}$. For PMN-PT transducers, the largest value of d_{15} was $2850 \times 10^{-12} \text{ m/V}$. Hence the maximum displacement, for a PMN-PT transducer at room temperature, e.g. for 150 V, is $\Delta L = 4.3 \times 10^{-7} \text{ m}$. The value of $\frac{\Delta L}{L} = 1.43 \times 10^{-3}$ which satisfies the condition that $\frac{\Delta L}{L} \ll 1$. We used the maximum excitation voltage of the capacitance bridge (15 V) to measure the capacitance changes between two blocks. The average time for each data point was set to 9 seconds on the capacitance bridge. The resolution of the capacitance bridge is $\frac{\Delta C}{C} = 5 \times 10^{-7}$ for a single measurement. This would give

a resolution in displacement (Δx) equal to 0.15 nm for typical spacing $L \sim 0.3$ mm. This can be compared to the displacement for LiNbO_3 which is $\simeq 2.4$ nm for lowest temperature $d_{15} = 6 \times 10^{-11}$ m/V and $\Delta V = 40$ V. The expected noise level would be $\simeq \frac{0.15 \text{ nm}}{2.4 \text{ nm}} \simeq 6\%$ for a single measurement. The actual noise level, we can see from the lowest temperature data for LiNbO_3 , is $\simeq \frac{3 \times 10^{-13}}{6 \times 10^{-11}} \simeq 0.5\%$. The reduction in noise ($\sim 10x$) came from data averaging. We averaged 50 readings for ± 20 V.

Chapter 4

Measurement of the piezoelectric coefficient d_{15}

This chapter describes the acquisition and analysis of the data which we used to investigate the temperature dependence of the piezoelectric coefficient d_{15} . Polycrystalline PZT and single crystals of PMN-PT and LiNbO_3 were investigated from room temperature down to 1.3 K. We discuss the analysis for each of these transducers in separate sections.

4.1 PZT polycrystalline ceramic shear transducers

A PZT-5A type rectangular transducer with gold electrodes from Boston Piezo Optics was used as a polycrystalline ceramic. The shape and dimensions are shown in Fig. 4.1. The measured dimensions of the transducer were $12.77 \times 9.58 \times 1.78 \text{ mm}^3$. The shear resonance frequency of the transducer is roughly 500 kHz.

A very simple scheme was used to acquire the data. A voltage V applied across the two electrodes of transducer created a shear deformation (since the polarization is parallel to the plane of the transducer). This deformed the

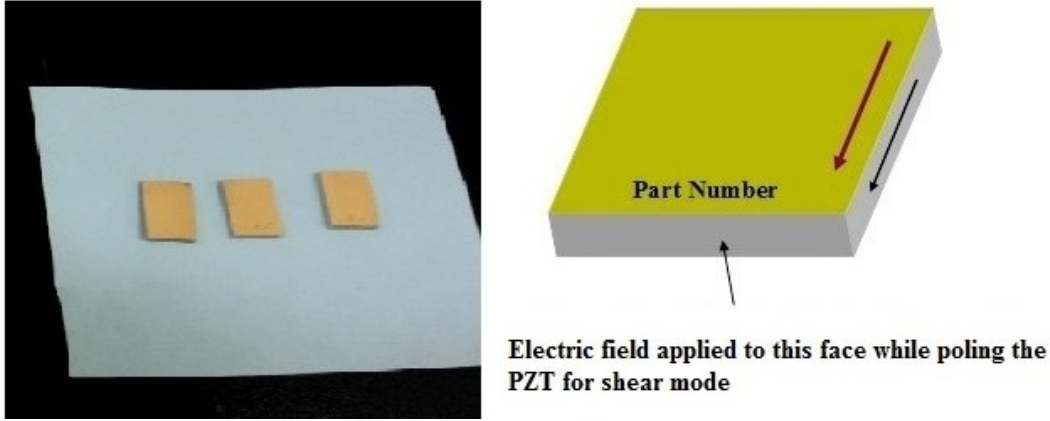


Figure 4.1: Photo and schematic of the PZT-5A shear transducers. Black arrow shows the direction of polarization for the shear transducers shown in left of the figure.

crystal and hence the magnetically clamped capacitor block moved forward and backward depending upon the polarity of the voltage. We applied a ± 20 V square wave voltage, with the shift in polarity after taking four data points and averaging the capacitance for about 12 seconds for each data point. Capacitance vs. time is shown in left of Fig. 4.2. The capacitance remains almost constant for each voltage, with noise much smaller than the signal. This particular data is for 20 K. The voltage vs. capacitance is plotted in Fig. 4.3 in order to determine the value of d_{15} . The straight line connects the average of all the data points for 20 V and -20 V. This would allow us to calculate the average capacitance, the average capacitance change and the average voltage change which are to be used to determine the average value of d_{15} for a particular temperature. We used similar method to obtain the other data points starting from room temperature down to the lowest possible temperature i.e. 1.3 K. The area of the capacitanc block was 14.08×14.40 mm².

The complete picture of the temperature dependence of d_{15} for PZT is given in Fig. 4.4. We can see that the value of d_{15} decreases almost linearly with the temperature. The values of d_{15} were almost independent of pressure of helium inside the vacuum can. We used helium exchange gas for most of

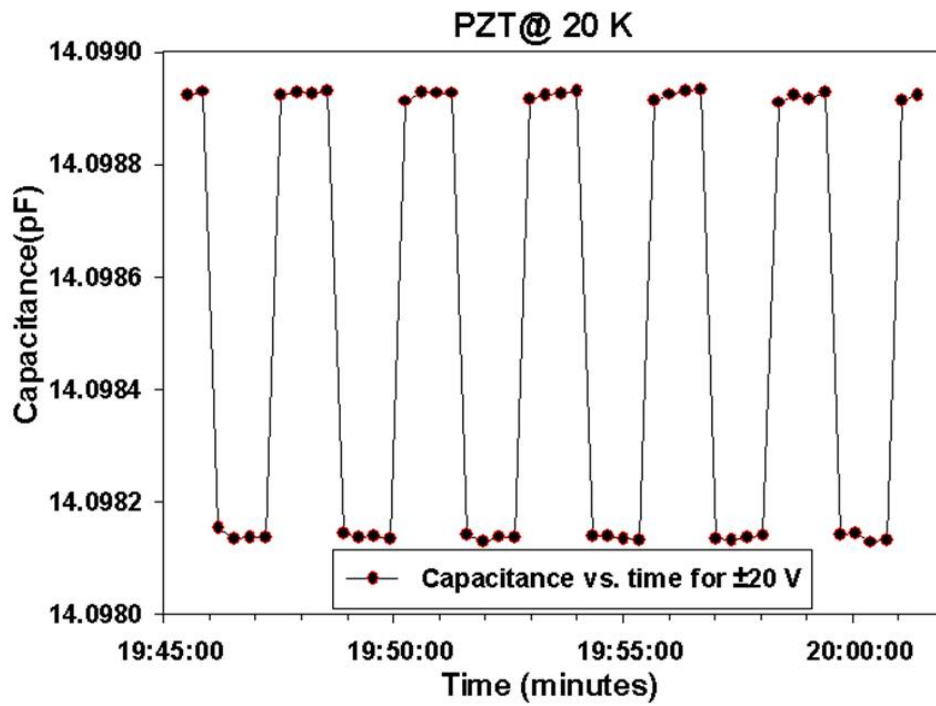


Figure 4.2: The change in capacitance induced by the deformation of PZT-5A across the parallel plate capacitor with change in applied voltage to the transducer.

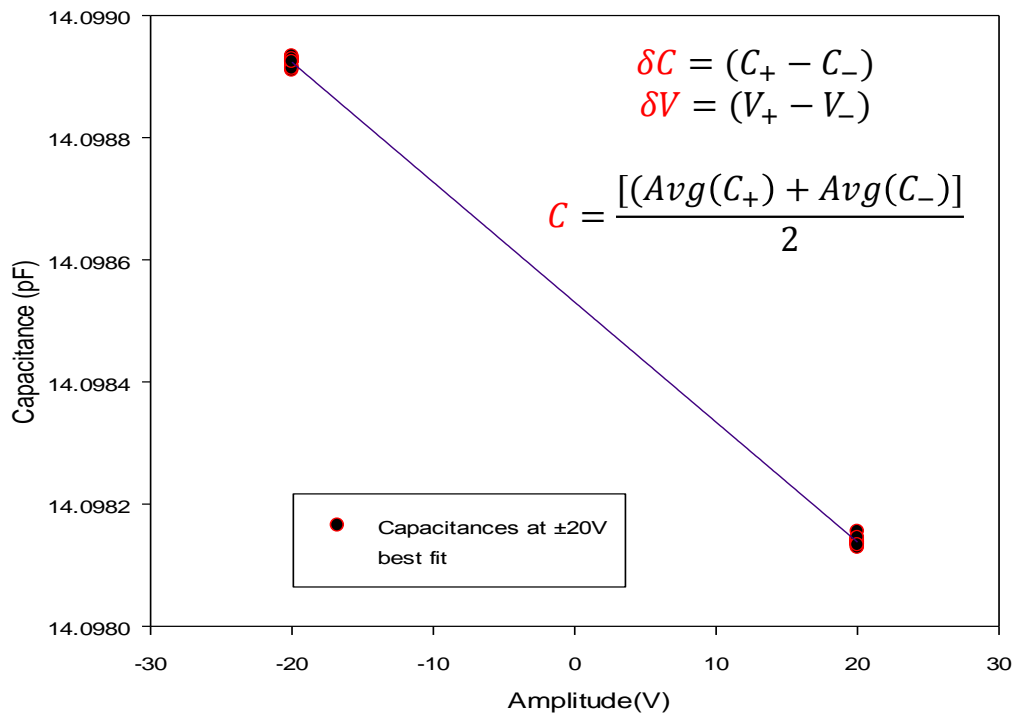


Figure 4.3: A best fit data shown was used to calculate the value of average capacitance or the value of capacitance at 0 V. The mathematical formulas for calculation of d_{15} are also shown.

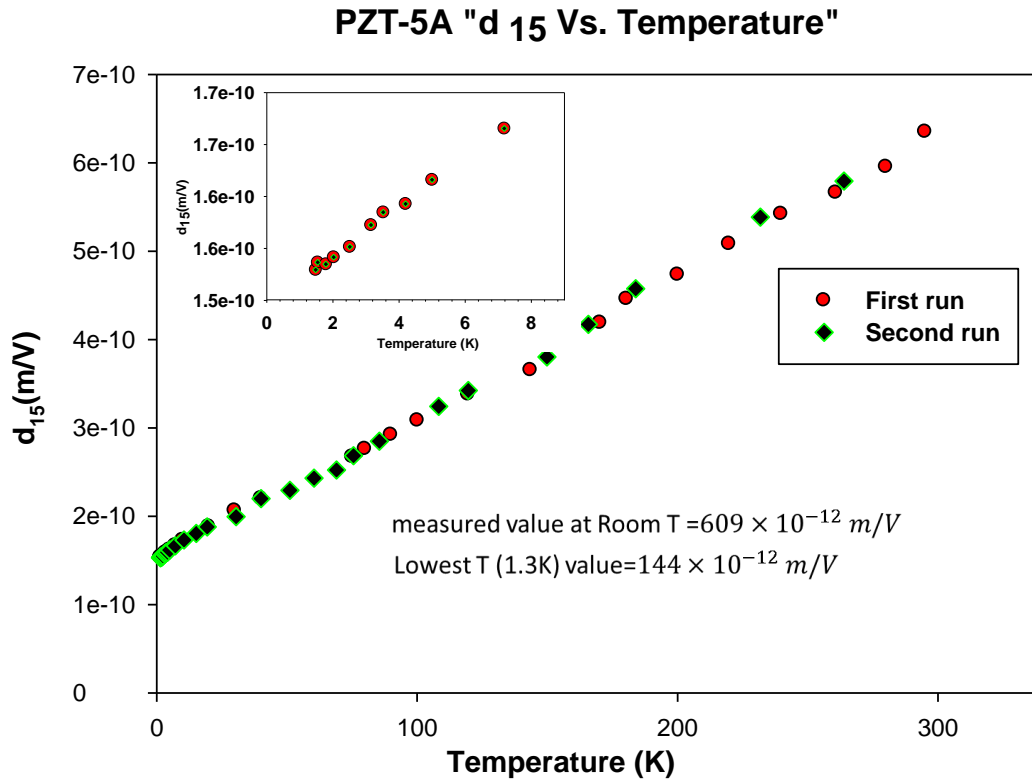


Figure 4.4: Temperature dependence of d_{15} shows the decrease in its magnitude with temperature, green diamonds show the data taken during the cooling while the red circular points show the data while warming up the cryostat. Inserted blow up shows the data below 10 K.

the measurements between (300-4) K and had to pump out the exchange gas to attain temperatures lower than 4 K. The data is nearly reproducible as two data sets were taken during cool down and warming up of cryostat.

The manufacturer quoted value for PZT transducers was 585×10^{-12} m/V at room temperature compared to our measured value of 609×10^{-12} m/V. This difference could be because we used a different experimental technique i.e. the capacitance measurement technique which could be affected by the stray capacitance. We will talk later about the stray effect and see if it really affects our measurements. The best fit for our data is given in Fig. 4.5. The lowest temperature (estimated) for these measurements is 1.3 K. The value of d_{15} dropped down to 144×10^{-12} m/V at this lowest temperature i.e. to a value 4.2 times smaller than its room temperature value. The decrease of d_{15} with temperature continued to the lowest temperature and would be very interesting to see this trend in mK range of temperatures.

The relation between the capacitance change and applied voltage is found to be linear at low temperatures. The voltage was varied in steps of 1 V per 60 seconds for ± 20 V ramps and 5 V per 60 seconds for ± 150 V. We did not see any hysteresis for voltages between +20 V and -20 V, as shown in Fig. 4.6. We raised the temperature to 1.8 K but did not see any hysteresis even for large values of applied voltages from +150 V to -150 V as shown in Fig. 4.7. The linearity of capacitance change over a wide range of voltages makes these transducers a good candidate to be used for measuring low temperature shear modulus changes in this temperature range. However the value of d_{15} was continuously decreasing, reducing the low temperature sensitivity of PZT-5A type transducers.

If we look at the phase diagram of PZT (see Fig. 2.11), the slope of MPB tells that the PZT-5A transducers are made from compositions near to the MPB to give maximum piezoelectric properties but this composition does not remains the correct one when we decrease the temperature, since the MPB

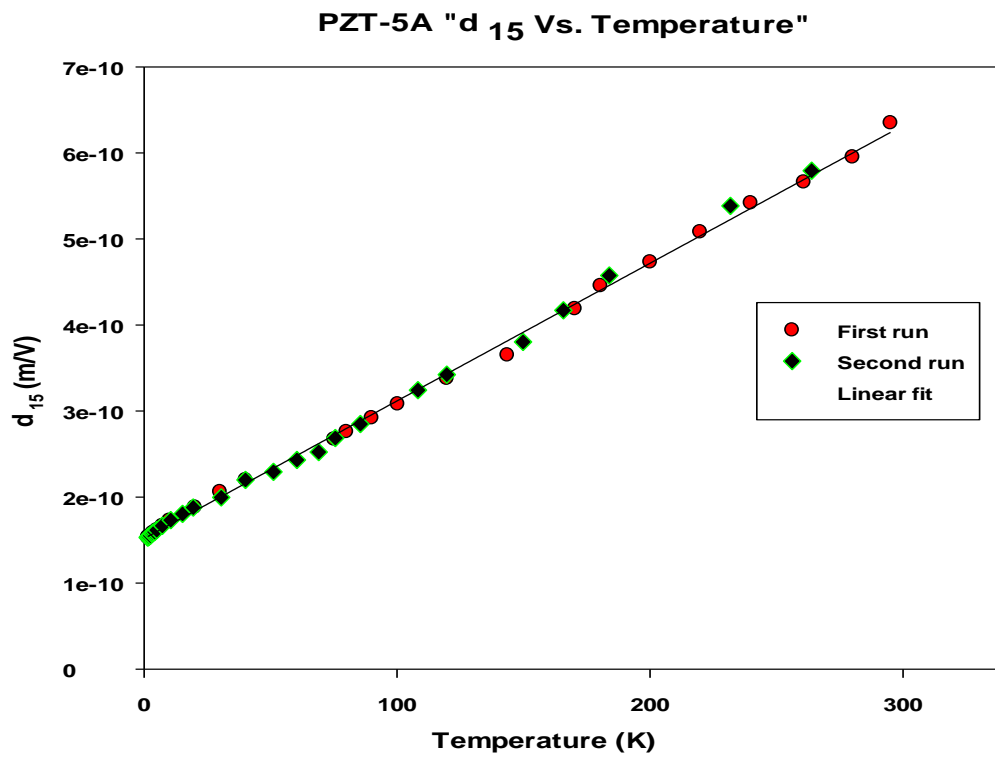


Figure 4.5: Linear fit of d_{15} vs. temperature. Data were taken during cooling (green diamonds) and warming (red circles) of the cryostat.

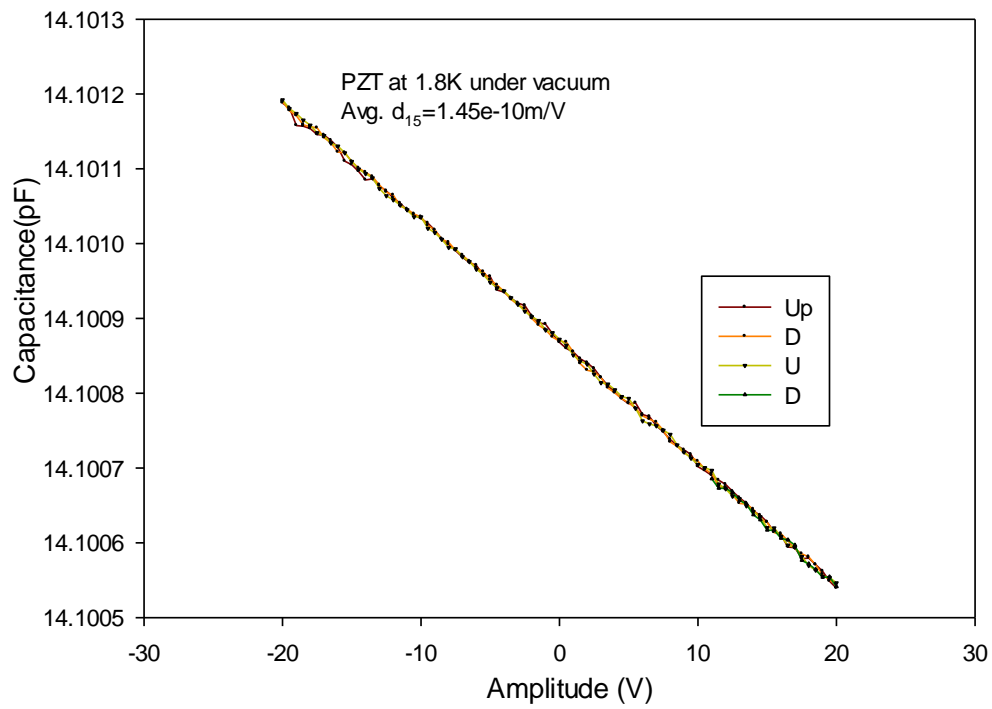


Figure 4.6: Voltage ramping at 1.8 K for ± 20 V with ramping rate of 1 V/minute.

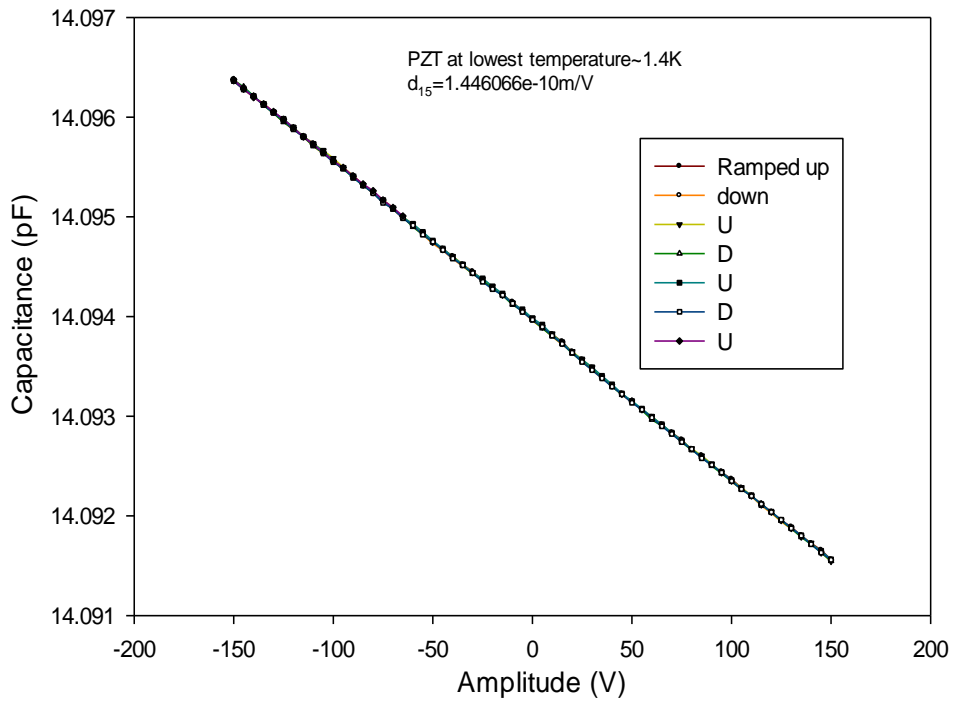


Figure 4.7: Linear piezoelectric behavior at 1.4 K for a voltage ramp of ± 150 V with ramping rate of 5 V/minute. No hysteresis observed even for large voltages.

shifts with temperature. We would need to fabricate transducers having a chemical composition near to the MPB at lower temperatures to maximize the piezoelectric response at low temperatures. Another aspect of the decreasing piezoelectric behavior can be linked to external contributions to ferroelectrics at high temperatures. These external factors like domain walls motion within grains and thermal contraction, can also effect piezoelectric properties [41, 40, 37].

4.2 Poled single crystals of PMN-PT

We used the same jig for PMN-PT transducers but with different blocks having slightly different area ($14.04 \times 14.34 \text{ mm}^2$) of capacitance plates. The dimensions of the transducers were $10 \times 10 \times 1 \text{ mm}^3$. The temperature dependence of d_{15} for PMN-PT single crystal transducer is given in Fig. 4.8. At high temperatures $>240 \text{ K}$, the temperature dependence of d_{15} is small but still significant as compared to the plateau region (90-240 K), where d_{15} is essentially independent of temperature. Similar studies were done for d_{33} and d_{31} of single crystals of PMN-PT by Martin et al. in 2012 between room temperature and 4 K [29]. The temperature dependence of d_{31} and d_{33} along with κ_{33} and κ_{31} is shown in Fig. 2.9. Their plateau region has still a moderate temperature dependence as compared to what we have observed. This might be related to the different measurement techniques (they used the resonance method), different polarization directions and strengths of the piezoelectric moduli in different directions along with chemical compositions of the samples.

We did not see any hysteresis when ramping the voltage at the lowest temperature which we estimate as 1.3 K. The lowest temperature voltage ramp is shown in Fig. 4.9. The applied voltage was varied from 150 V to -150 V and vice versa. The observed linear behavior and lack of hysteresis for high voltages would lead to the conclusion that these transducers are a good choice for low

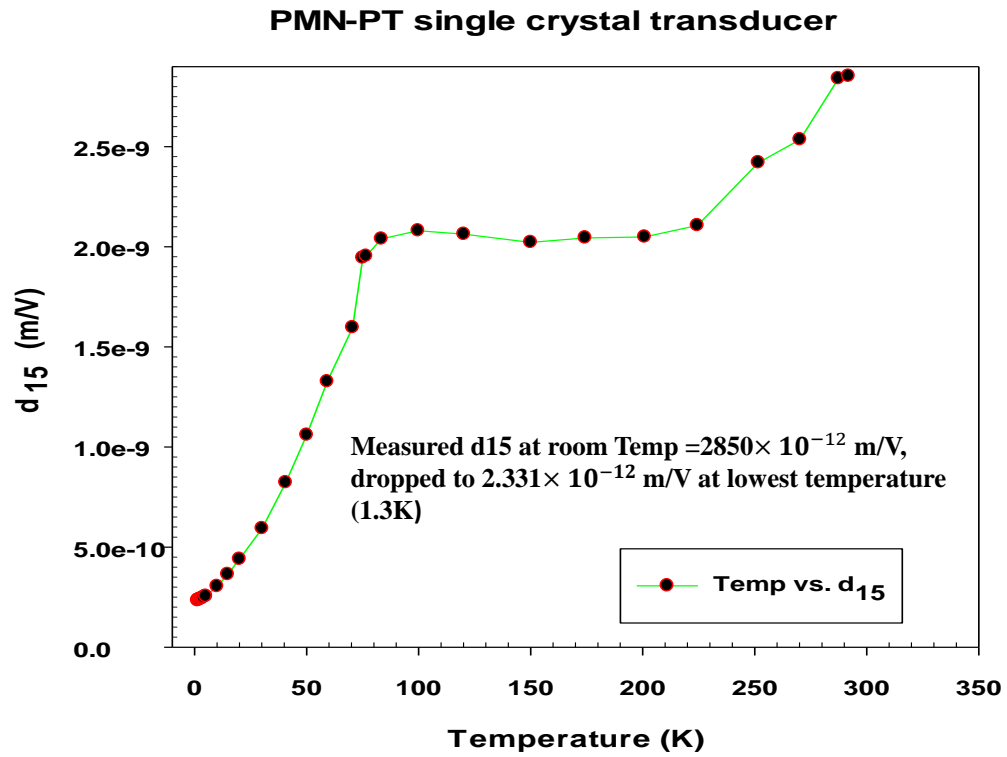


Figure 4.8: The temperature dependence of d_{15} from room temperature down to lowest temperature i.e. 1.3 K. The high temperature, plateau (90-240 K) and low temperature regions have clearly different temperature dependences.

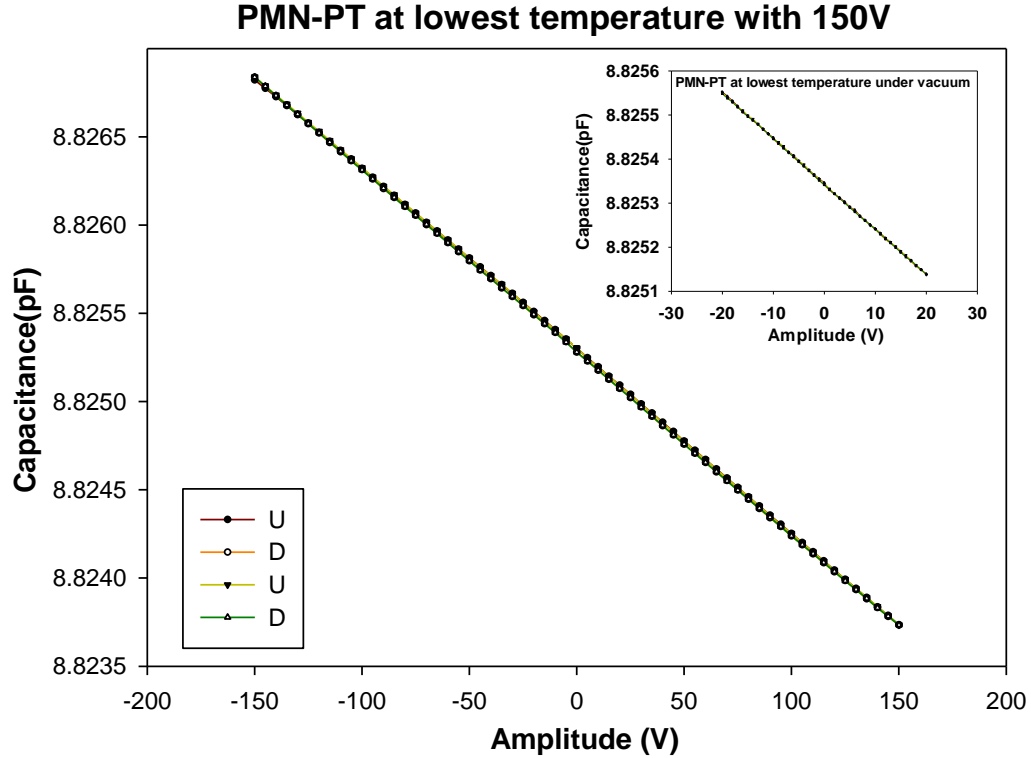


Figure 4.9: The linear relation between capacitance and applied voltage both for large and small strains. Voltage was ramped at 5 V/ minute. The absence of hysteresis at low temperature is important from the application point of view in this temperature range.

temperature elastic constant measurements of solid helium over a wide range of applied stresses. This is also a good candidate for low temperature STMs.

The linear relation between the applied voltage and the observed capacitance was observed at 4 K as well, when the voltage was varied between ± 20 V. No hysteresis means the switching of electric field direction does not affect the polarization at this temperature (see Fig. 4.10). This might be due to the freezing of the domain boundaries, resulting in a pure polarization effect in this temperature range.

As we raised the temperature to 78 K i.e. to liquid nitrogen temperature, the voltage vs. capacitance relation developed hysteresis. We observed hysteresis both for large (± 150 V) and small (± 20 V) voltages. The hysteresis is shown in

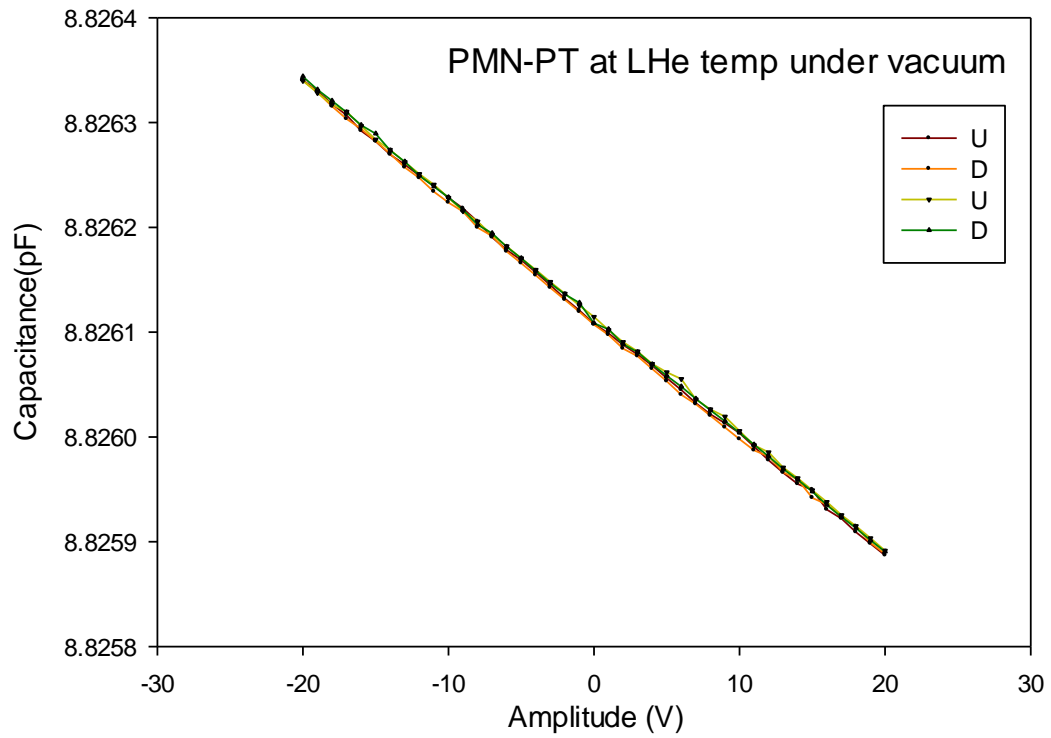


Figure 4.10: There is no hysteresis even at liquid helium temperature (4 K). The data was taken for small stresses i.e. ± 20 V. The voltage was varied in steps of 1V every 60 seconds.

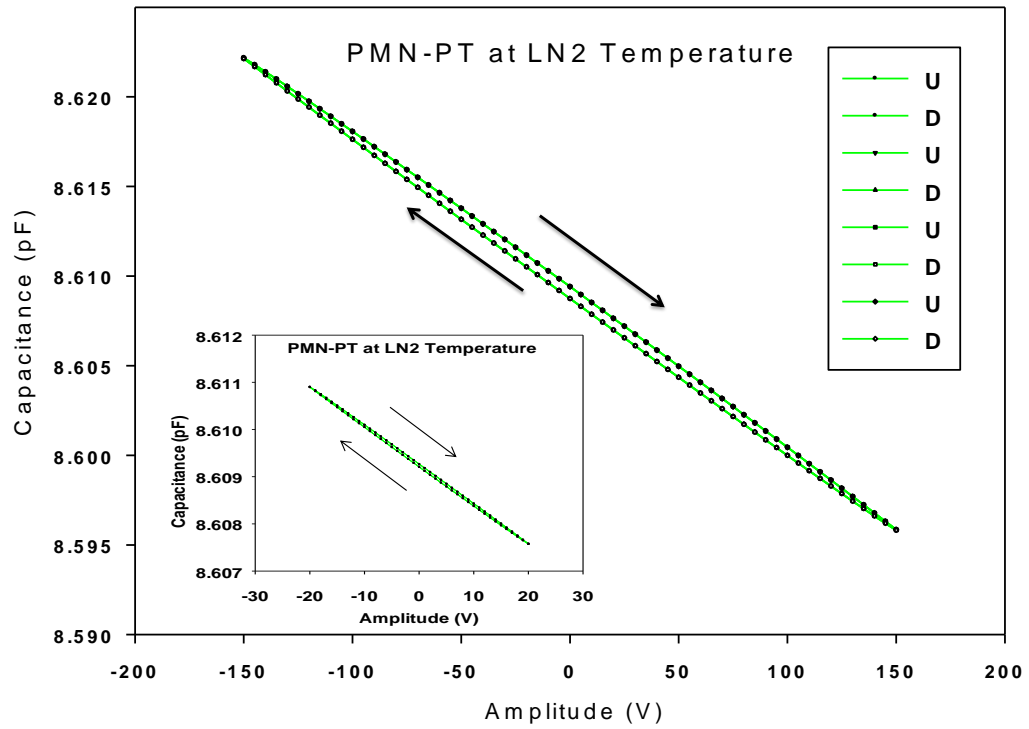


Figure 4.11: Hysteresis at LN₂ temperature both for small ± 20 V and large ± 150 V applied voltages. The voltage was varied in steps of 5 V every 60 seconds.

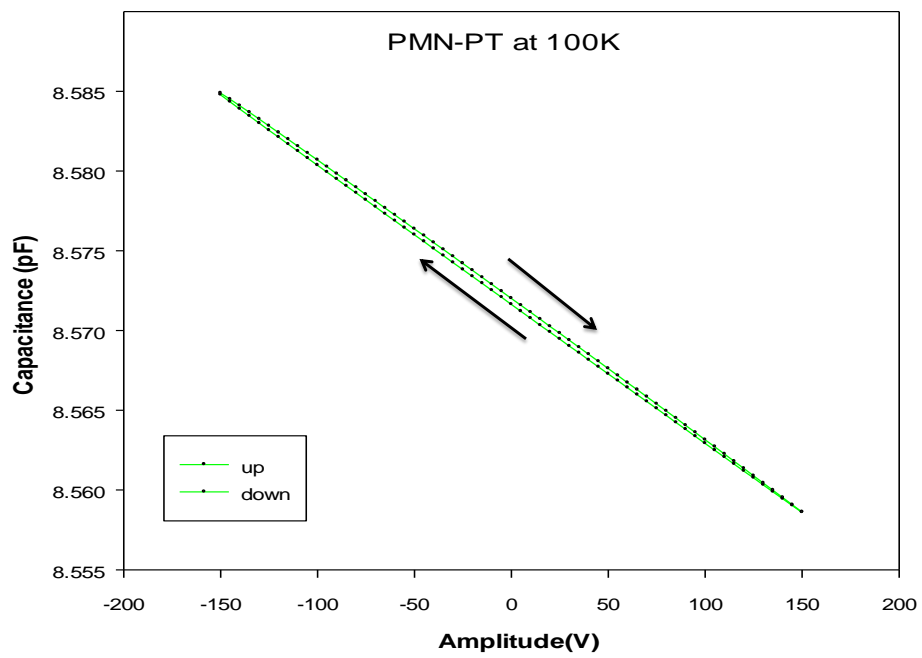


Figure 4.12: Similar hysteresis observed at 100 K as we saw at 78 K. The voltage was varied in steps of 5 V every 60 seconds.

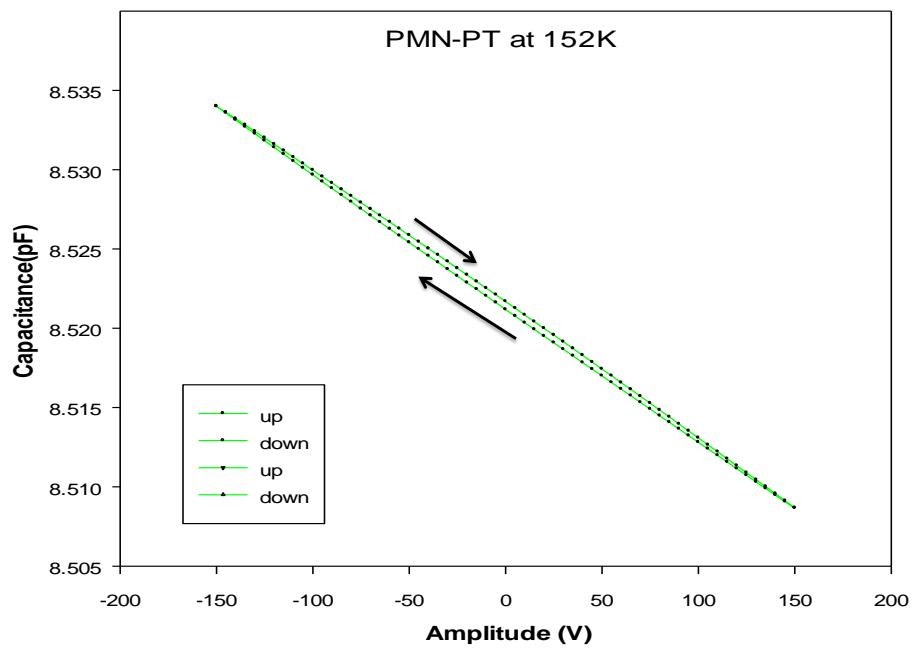


Figure 4.13: Hysteresis at 152 K for ± 150 V. The voltage was varied in steps of 5 V every 60 seconds.

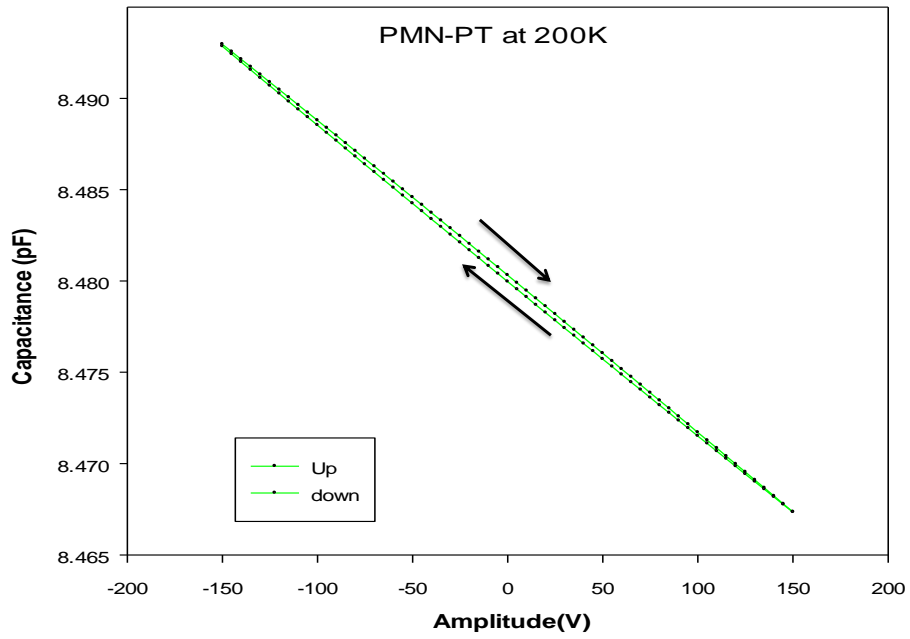


Figure 4.14: Hysteresis at 200 K for ± 150 V. The magnitude of hysteresis is quite similar to what we observed at 152 K, 100 K and 78 K. We used similar voltage ramping rate as we used in previous cases i.e. 5 V every 60 seconds.

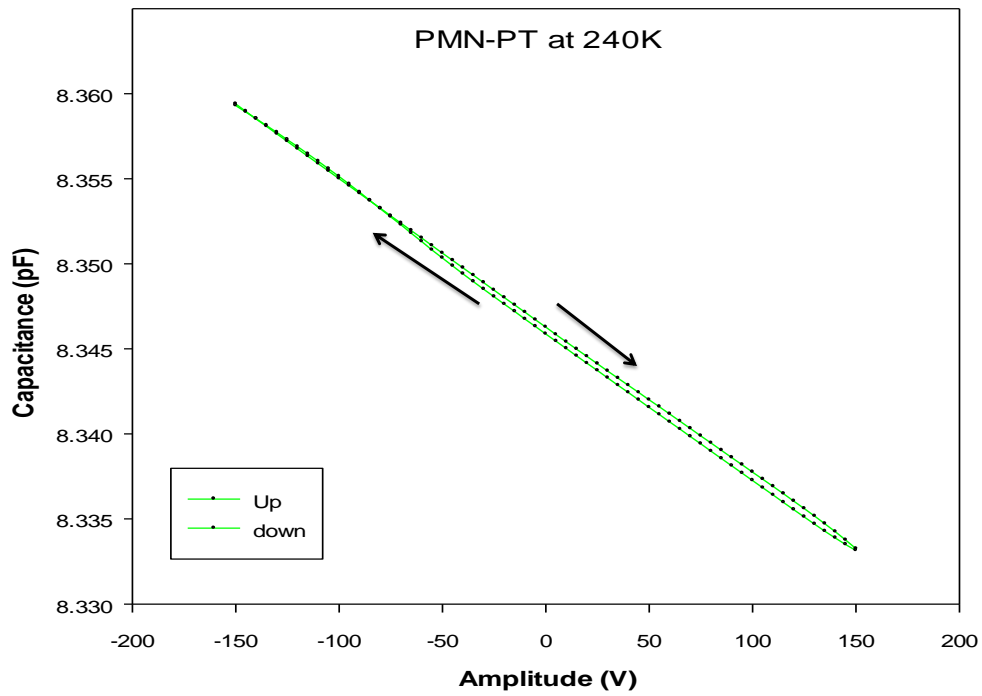


Figure 4.15: The hysteresis curve started changing its shape. It looks like the high strains on transducer started effecting the polarization of the transducer. Voltage ramped 5 V every minute.

Fig. 4.11. At higher temperatures, the contribution of domain boundaries and inter-granular regions probably increases the magnitude of piezoelectric modulus d_{15} and produces hysteresis in the voltage-capacitance relation. Hysteresis appears at a temperature when domain walls are no longer frozen and start moving with applied voltages.

Further increase in temperature revealed similar hysteresis loops at 100, 152 and 200 K. Since there was hysteresis for small voltages at LN₂ temperature, we only ramped the voltage to $\pm 150V$ to check whether we saw similar effects which we observed at liquid nitrogen temperature. The magnitude of the hysteresis remained almost same which gives us a clue that the hysteresis effect remains independent of temperature over a large temperature window, once it turned on somewhere between 4 and 78 K.

The shape of hysteresis changed at 240 K, see Fig. 4.15. The drift in the hysteresis curve could be just the temperature changes as its a bit harder to control the temperature above 200 K.

4.3 Single crystal LiNbO₃

A relatively thin sheet of single crystal of lithium niobate ($10.04 \times 10.05 \times 0.28$ mm³) was used in current study. The area of the capacitance blocks was $13.95 \times 13.97 \times$ mm². The temperature dependence of d_{15} for lithium niobate is quite different than that of PZT ceramics and PMN-PT single crystals. LiNbO₃ single crystals contain domains and domain boundaries like PMN-PT. They need to be polarized to exhibit piezoelectric character. They have a very high value of Curie temperature compared to other ferroelectrics. They can only be de-poled with high electric fields or temperatures (greater than 1410 K). When we pole the single crystal structure, the ions change their equilibrium position. The distorted phase could be either hexagonal or rhombohedral and both of these phases exhibit piezoelectricity. The crystal structure is non centro-

symmetric.

We did not expect a large change in d_{15} with decreasing temperature and that was what we observed. The value of d_{15} falls only by a factor of 1.07 compare to its room temperature value i.e. 64×10^{-12} m/V dropped to 60×10^{-12} m/V by the time we reach the lowest temperature. The observed behavior may be related to the thermal contraction of the crystals at low temperatures. This thermal contraction can potentially relocate the Li and Nb ions, changing the overall polarization of the crystal. The magnitude of the drop of d_{15} with temperature is however very small as compared to PZT and PMN-PT. The data looks a bit noisy but we did see similar temperature dependence for two transducers used in different cooling/heating cycles. The signal to noise ratio is small because the piezoelectric response of LiNbO_3 crystals is not comparable to the other piezoelectric sensors for which the increased piezoelectric behavior is observed because of chemical compositions, Curie temperatures, extrinsic effects, etc.

Voltage ramping at cryogenic temperatures did not show any hysteresis from room temperature down to the lowest temperatures for either experimental run. The data for cryogenic temperatures is shown in Figs. 4.17, 4.18, 4.19, and 4.20. The lack of hysteresis makes these transducers a good choice to replace PZT and PMN-PT in stack actuators, which would give temperature and voltage independent probes, for many low temperature applications where the temperature dependence is crucial.

Finally we plotted the temperature dependence of d_{15} for all three transducers as a function of temperature. The relative magnitudes in different temperature regions are quite clear and give a clear guidance when choosing a particular material to be used for cryogenic applications. The two PMN-PT curves are from measurements on two transducers from the same lot. Both follow the same trend as we change the temperature but the one we used in the first run had a bigger magnitude. The data between helium and liquid nitrogen

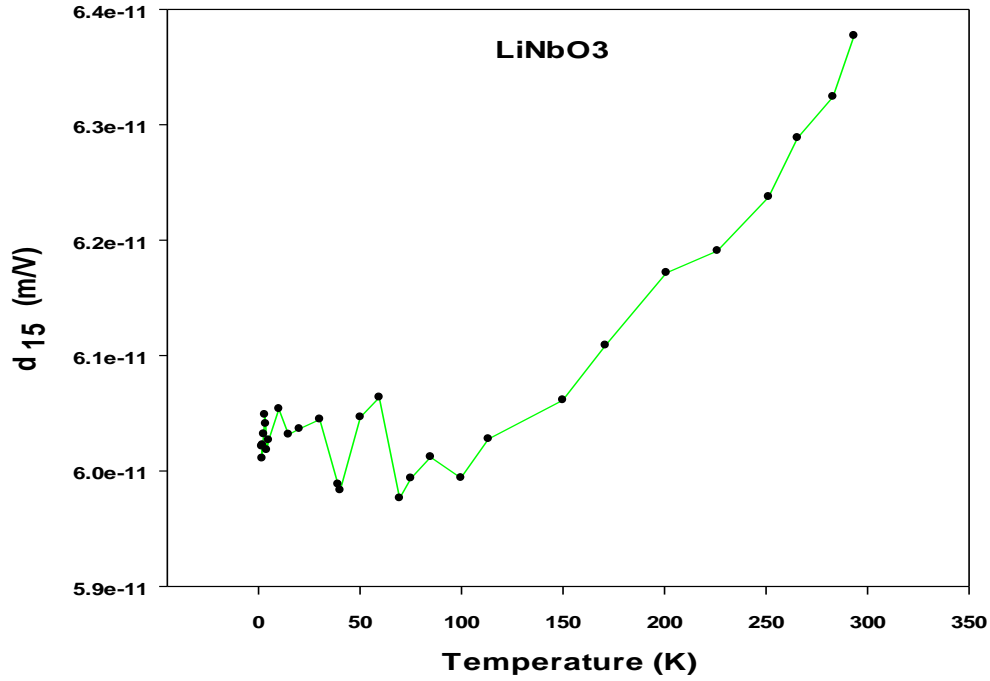


Figure 4.16: Temperature dependence of piezoelectric modulus d_{15} of 41^0 x-cut single crystals of lithium niobate. The lowest temperature value is only about 7% smaller than the room temperature which is very small as compare to that of PZT and PMN-PT. The expected noise level of capacitance bridge would correspond to a $\simeq 6\%$ variation in d_{15} for a single measurement. The actual noise level is smaller because of signal averaging, as we can see from the lowest temperature data here, i.e. $\simeq \frac{3 \times 10^{-13}}{6 \times 10^{-11}} \simeq 0.5\%$.

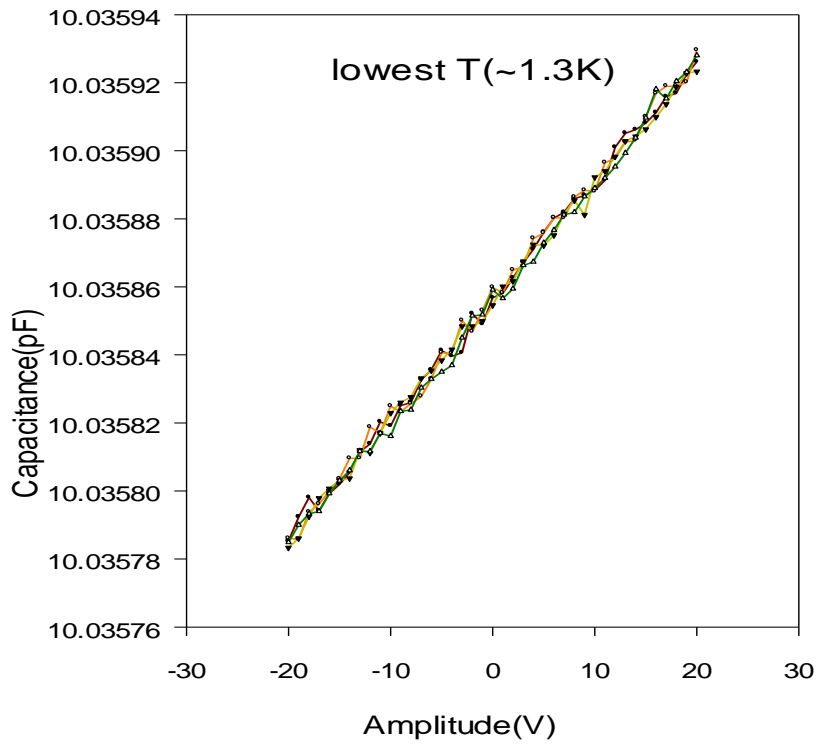


Figure 4.17: No hysteresis observed for lithium niobate single crystals for lowest temperature and small applied strains. The ramping rate was 1 V per 120 seconds.

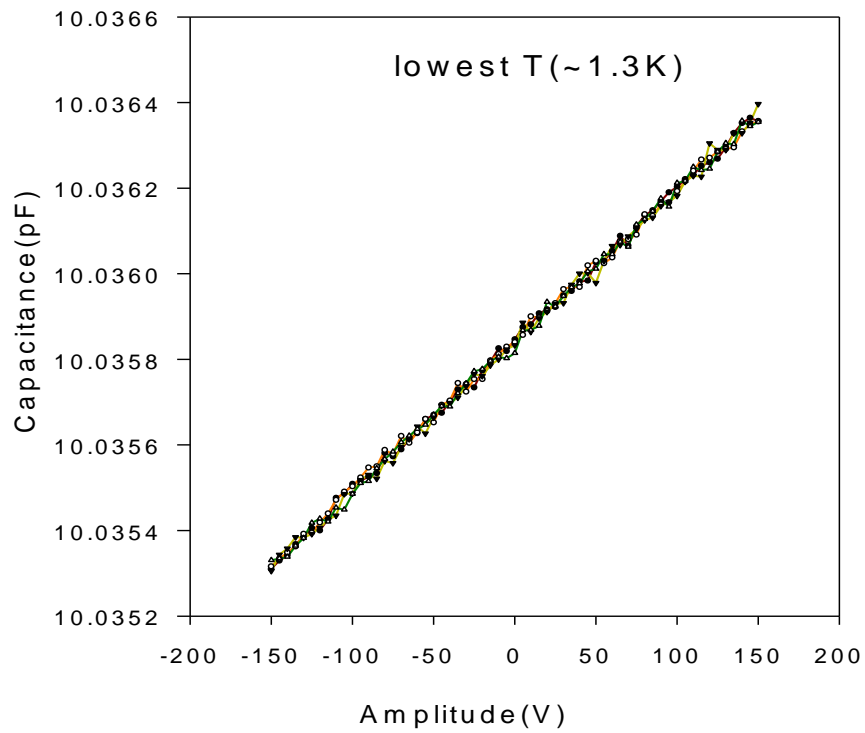


Figure 4.18: Capacitance vs. voltage for ± 150 V for at 1.3 K. No hysteresis as expected for lithium niobate single crystals. The ramping rate was 5 V per 120 seconds.

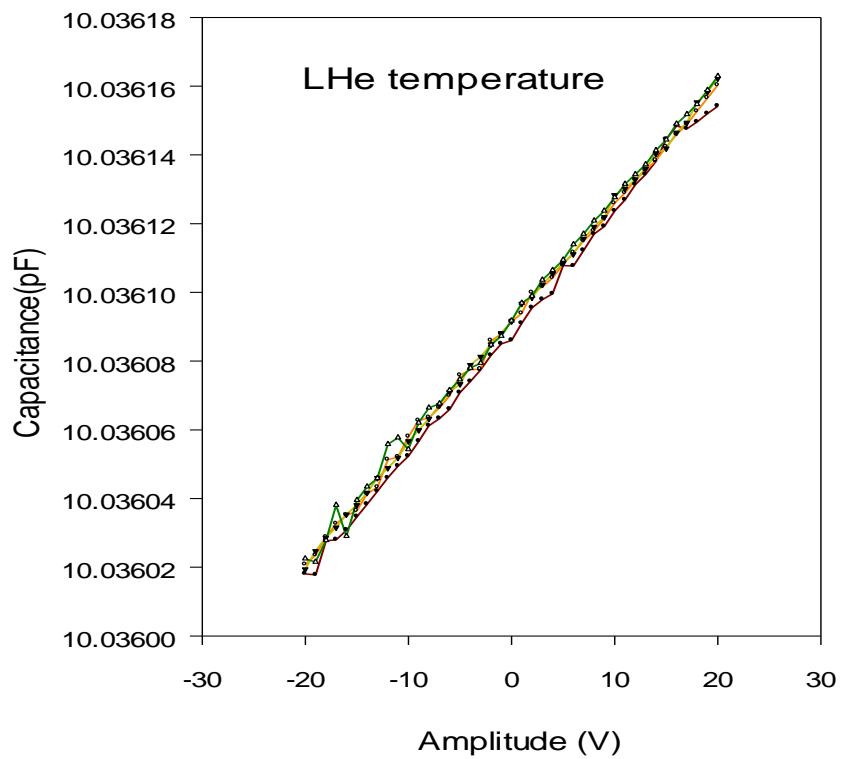


Figure 4.19: Hysteresis curve is reproducible at 4 K. The ramping rate was 1 V per 120 seconds.

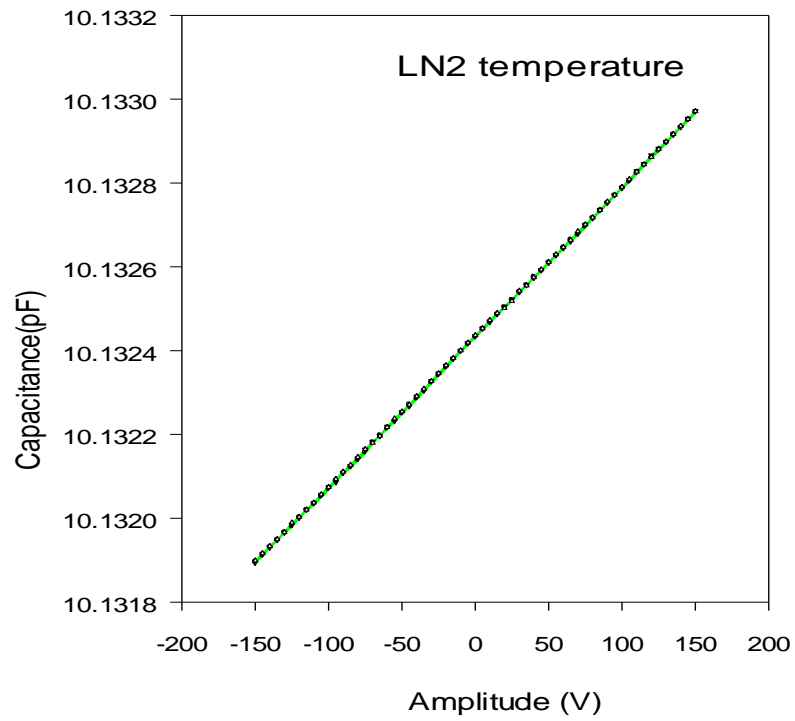


Figure 4.20: Voltage ramp: 5 V per 120 seconds at 78 K.

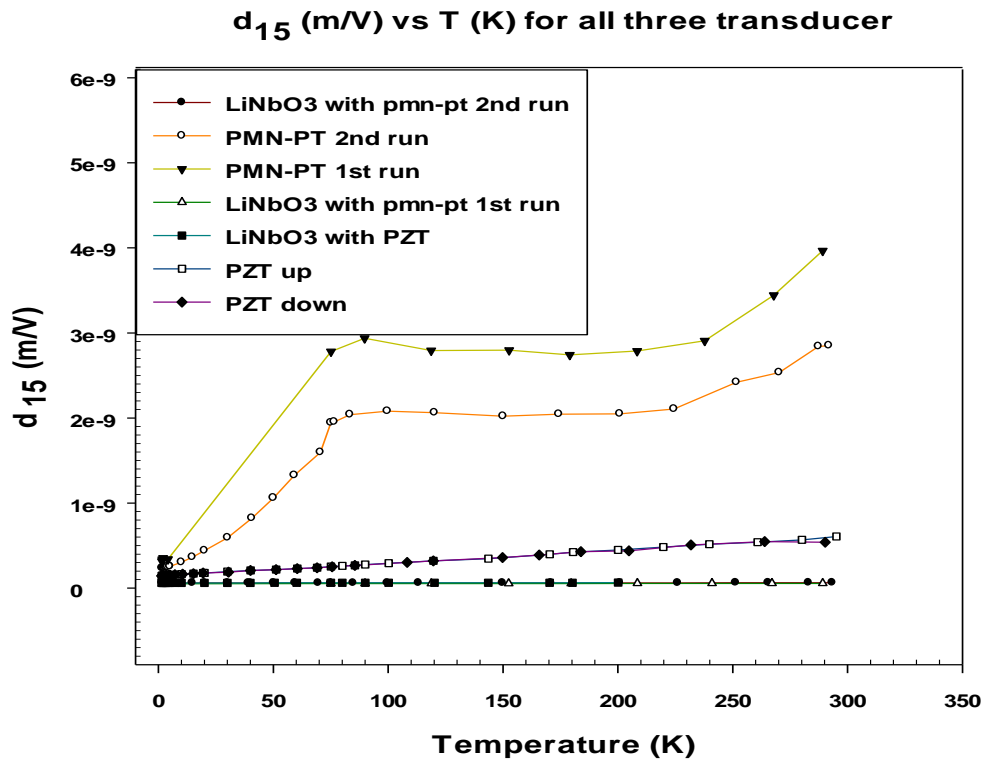


Figure 4.21: The data for all three types of transducers we studied show a relative change in magnitude of the piezoelectric modulus d_{15} from room temperature down to lowest temperature.

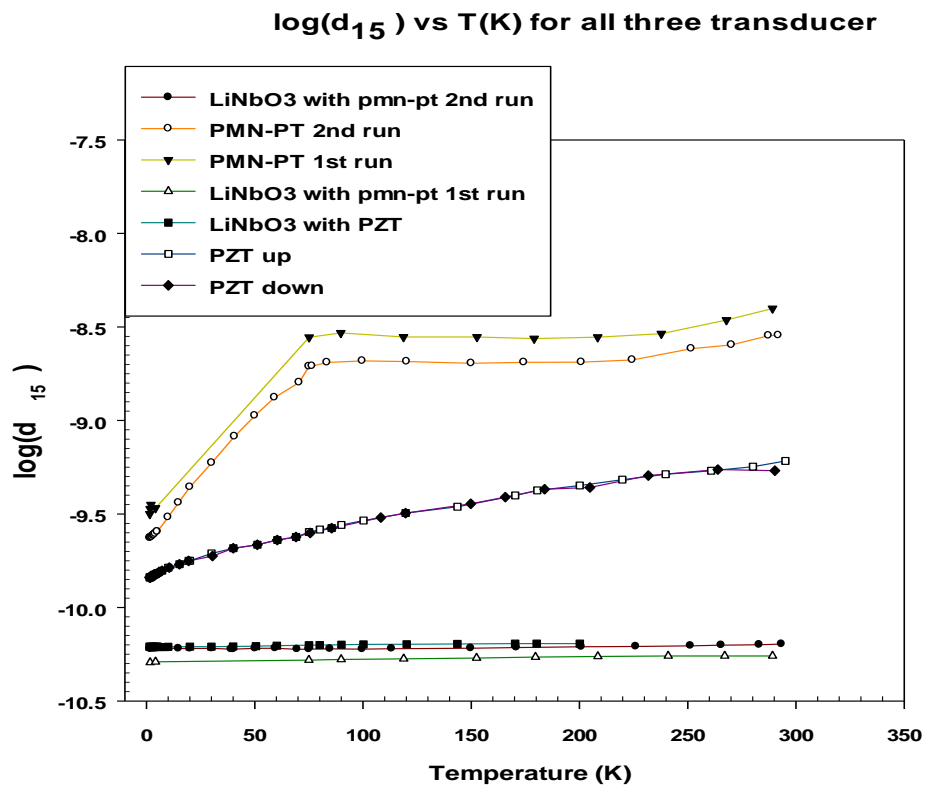


Figure 4.22: The $\log(d_{15})$ vs. temperature gives a clear view of the behavior of d_{15} at low temperatures.

temperature is missing for one transducer because the solder was broken and voltage wire came off from the transducer. We expect the same trend in this region as we have lowest temperature data, which is quite similar for both.

4.4 Conclusions

Knowledge of the shear piezoelectric coefficients at cryogenic temperatures is important because of applications in modern STM, AFM, and other actuators and receivers being used at low temperatures. The understanding of the behavior of these moduli with temperature would help choosing a particular material from the range of piezoelectric elements being fabricated and used commercially these days. Our study is limited to the pure shear mode piezoelectric modulus d_{15} of three of the best known and most promising materials, ceramic PZT, polarized single crystals of PMN-PT and single crystals of lithium niobate transducers.

We observed a nearly linear decrease in d_{15} for the PZT ceramic transducer PZT-5A between room temperature and 1.3 K. Voltage ramps did not show any hysteresis at 1.4 K or 1.8 K. We expect no hysteresis below 1 K, which would allow us to use large voltages and deformations to study the plastic deformation of helium solids at mK temperatures. The value of d_{15} dropped by 4.2 times and continued dropping at the lowest temperature. This would suggest a smaller sensitivity at mK temperatures.

PMN-PT are polarized single crystals with the highest piezoelectric d_{15} observed at all temperatures. The value of d_{15} is not linearly dependent on temperature. It decreases from room temperature down to 240 K, then remains almost unchanged down to 90 K. We see a sharp drop in d_{15} below 90 K and it reaches a similar magnitude as that of PZT and lithium niobate below 4 K.

Single crystals of LiNbO_3 showed a small decrease in d_{15} from room temperature down to 150 K but no temperature dependence below this temperature.

We did not see any hysteresis for temperatures below liquid nitrogen temperature. The lowest temperature value of d_{15} is 60×10^{-12} m/V which is only 7% below its room temperature value. This would allow us to fabricate an actuator with relatively high piezoelectric coefficient and no hysteresis at low temperatures.

Chapter 5

Summary

Finally we, summarize our results with suggestions for future directions in the study of temperature dependence of piezoelectric coefficients at cryogenic temperatures. We will discuss the three types of transducers in separate sections. Our studies were done mainly to understand the sensitivity of these transducers at low temperatures, which would help studying the elastic properties of single crystal and polycrystalline solid helium in the millikelvin range.

We used a direct displacement measuring technique to determine the piezoelectric coefficient d_{15} . The transducers were magnetically clamped to a brass jig with a fixed and a movable brass block. When we applied a voltage on the transducer, it generated shear strain in it and moved the brass block clamped to it. Two capacitance leads were used to measure the capacitance changes using a high resolution AH capacitance bridge. The value of d_{15} was calculated using the relation between voltage, capacitance and the distance between the plates.

5.1 Summary of lithium niobate

Single crystals of 41^0 X-cut lithium niobate give the shear piezoelectric coefficient d_{15} when voltage is applied perpendicular to the direction of the po-

larization, Z. The data were taken for each temperature by measuring the capacitance changes for each applied voltage of ± 20 V. The calculated value of d_{15} was plotted versus temperature to see its dependence over a wide range (from room temperature down to 1.3 K). The coefficient d_{15} decreased by approximately 6% by the time temperature reached 150 K. We did not see any noticeable variation in d_{15} below that temperature down to 1.3 K. We saw some fluctuations in the data but those were prominent only because the signal to noise ratio was quite small. The piezoelectric response of these crystals appeared because of the poling of the single crystals near the Curie temperature and hence obtained the piezoelectric character. The changes in d_{15} with temperature might be associated with the relocation of the ions responsible for dipoles inside the crystal and hence the polarization. This could be possible because of the thermal expansion/contraction of the crystal with cooling. This thermal expansion could cause anharmonic effects in the crystal distorting the tetragonal structure causing a net decrease in the piezoelectric modulus d_{15} .

5.2 Summary for PMN-PT

PMN-PT ferroelectrics exhibit the highest values of piezoelectric moduli at room temperature. They are very fragile at low temperatures, as we have experienced a few times when we cooled them below 4 K to measure the elastic moduli of solid helium here in our lab and at ENS in Paris. Whenever we tried to epoxy them to a brass or copper metallic plate, they were broken during cooling. This suggested that they contract a lot when they are cooled. We did not have an optical set up to see how much their dimensions changed with temperature but we did notice their piezoelectric response changed a lot with cooling.

The temperature vs. d_{15} curve is divided in three sections. The first section is a region of moderate dependence of d_{15} on temperature from room tempera-

ture down to 240 K. The observed decrease might be due to the disappearance of extrinsic effects in the piezoelectric modulus which are predicted to be present only at high temperatures. The plateau region where the value of d_{15} is almost independent of temperature changes extends from 240 to 90 K . This is a region which may be useful for space applications which often operate in this temperature range. The last region shows the fastest drop in d_{15} with temperature. This region covers liquid nitrogen and helium temperatures and extends down to our lowest temperature (1.3 K). The sudden drop in piezoelectric modulus can be attributed to the disappearance of the inter-domain boundary effects at low temperatures.

The MPB plays an important role in the selection of a particular composition for ceramic PZT and single crystals of PMN-PT. Careful choice of initial composition might help in getting higher values of the piezoelectric moduli at low temperatures but might reduce their values at room temperature.

5.3 Summary of PZT

Ceramic piezoelectrics are prepared with solid state reaction methods. The composition of the samples prepared is again selected from the phase diagram near the MPB for PZT ferroelectrics. We used PZT-5A type transducers which are polycrystalline and need to be polarized during the annealing process to get a net polarization in a particular direction. The crystals are polarized in the Z-direction for shear transducers and voltage is applied perpendicular to this polarization. These materials are being used in billion dollar industries in medical imaging, sonar, surface wave detectors, advance scanning probe tips, and in sensors and actuators to study the mechanical properties of solids.

We observed a linear drop in d_{15} over a temperature range from room temperature down to the lowest temperature obtained in the current run of our fridge. The decrease in piezoelectric modulus can be related to the MPB com-

position selection. If we see the composition being chosen for these type of transducers, we can see that the composition point lies near the phase boundary of the composition vs temperature diagram and is selected for maximum high temperature piezoelectric response. This point would move a bit away from the MPB upon cooling, causing the suppression in the piezoelectric modulus. We suggest to select the composition in such a way that the low temperature value of d_{15} is maximized even if the high temperature value is smaller.

The piezoelectric response coming from inter-grain effects also decreased at lower temperatures because of reduced extrinsic contributions. The piezoelectric response of these transducers is, however, found to be linear over a wide range of voltages.

5.4 Future directions

The piezoelectric coefficient d_{15} for LiNbO_3 does not change much below room temperature. This modulus at the lowest temperature is comparable to that of PZT and PMN-PT. We propose to fabricate a stack of these transducers as a piezoelectric actuator which would have large piezoelectric moduli and high sensitivity for low temperature measurements. It is easier to fabricate reasonably sized actuator with a large number of thin transducer sheets since lithium niobate can be cut into very small slices after being polarized. This would help us to make a compact actuator. Actuators could be made to measure d_{33} , d_{31} and d_{15} over a wide range of temperature.

We saw a decrease in d_{15} both for PZT and PMN-PT transducers, down to the minimum temperature we achieved in our 1 K fridge. We are planning to study actuators and single transducers over a wide range of temperature, down to 20 mK so that we have a better understanding of their behavior in the temperature range where we plan to do further experiments to study the mechanical properties of the solid ^4He and ^3He .

Bibliography

- [1] University of Cambridge. <http://www.doitpoms.ac.uk/tlplib/ferroelectrics/dipole.php>. DoITPoMS, TLP library.
- [2] Antonio Arnau Vives and Antonio Arnau. *Piezoelectric transducers and applications*. Springer, 2008.
- [3] Gene. H. Haertling. Ferroelectric ceramics: history and technology. *Journal of the American Ceramic Society*, 82(4):797–818, 1999.
- [4] Kenji Uchino. Introduction to Piezoelectric Actuators and Transducers. Technical report, DTIC Document, 2003.
- [5] Akito Kawamata, Hiroshi Hosaka and Takeshi Morita. Non-hysteresis and perfect linear piezoelectric performance of a multilayered lithium niobate actuator . *Sensors and Actuators A: Physical*, 135(2):782 – 786, 2007.
- [6] S.O. Reza Moheimani and Andrew J. Fleming. *Piezoelectric Transducers for Vibration Control and Damping*. Springer London, 2003.
- [7] Han J. M. T. A. Adriaens, Willem L. de Koning, and Reinder Banning. Modeling Piezoelectric Actuators. *IEEE/ASME Transactions on Mechatronics*, VOL 5, NO. 4,:331–341, DECEMBER 2000.
- [8] Jayant Sirohi and Inderjit Chopra. Fundamental understanding of piezoelectric strain sensors. *Journal of Intelligent Material Systems and Structures*, 11(4):246–257, 2000.

- [9] J F Nye. *Physical Properties of Crystals: Their Representation by Tensors and Matrices*. Oxford University Press, 1985.
- [10] Srinivasan, T. P. Invariant Piezoelectric Coefficients for Crystals. *Physica Status Solidi (b)*, 41(2):615–620, 1970.
- [11] M. Levy, Jr. R. M. Osgood, R. Liu, L. E. Cross, G. S. Cargill III, A. Kumar, and H. Bakhru. Fabrication of single-crystal lithium niobate films by crystal ion slicing. *Applied Physics Letters*, 73(16):2293–2295, 1998.
- [12] Weis, R.S. and Gaylord, T.K. Lithium niobate: Summary of physical properties and crystal structure. *Applied Physics A*, 37(4):191–203, 1985.
- [13] V.Grachev G. Malovichko. Evolution of conception of intrinsic and extrinsic defects in lithium niobate. *Department of Physics, University of Osnabruck, Germany Fourth Annual Meeting of the COST Action P2 "Applications of nonlinear optical Phenomena" and Workshop on LiNbO3. Budapest, May 2001 (Invited talk).*, May, 2001.
- [14] Karsten Buse. Light research group. Bonn University.
- [15] Tomoaki Yamada, Nobukazu Niizeki, and Hiroo Toyoda. Piezoelectric and elastic properties of lithium niobate single crystals. *Japanese Journal of Applied Physics*, 6(2), 1967.
- [16] Sanna, Simone and Schmidt, Wolf Gero. Lithium niobate X-cut, Y-cut, and Z-cut surfaces from ab initio theory. *Physical Review B*, 81(21):214116, 2010.
- [17] R. T. Smith and F. S. Welsh. Temperature dependence of the elastic, piezoelectric, and dielectric constants of lithium tantalate and lithium niobate. *Journal of Applied Physics*, 42(6):2219–2230, 1971.

- [18] A. W. Warner, M. Onoe, and G. A. Coquin. Determination of Elastic and Piezoelectric Constants for Crystals in Class (3m). *The Journal of the Acoustical Society of America*, 42(6):1223–1231, 1967.
- [19] Hirotsugu Ogi, Yasunori Kawasaki, Masahiko Hirao, and Hassel Ledbetter. Acoustic spectroscopy of lithium niobate: elastic and piezoelectric coefficients. *Journal of Applied Physics*, 92(5):2451–2456, 2002.
- [20] Eugene V. Colla, Nikolai K. Yushin, and Dwight Viehland. Dielectric properties of $(\text{PMN})(1-x)\text{PT}(x)$ single crystals for various electrical and thermal histories. *Journal of Applied Physics*, 83(6):3298–3304, 1998.
- [21] Ursic Hana and Santo Zarnik, Marina and Kosec, Marija. $\text{Pb}(\text{Mg}_{1/3}\text{Nb}_{2/3})\text{O}_3 - \text{PbTiO}_3$ (PMN-PT) Material for Actuator Applications. *Smart Materials Research*, 2011, 2011.
- [22] Zhi-Wen Yin, Hao-Su Luo, Ping-Chu Wang, and Gui-Sheng Xu. Growth, characterization and properties of relaxor ferroelectric PMN-PT single crystals. *Ferroelectrics*, 229(1):207–216, 1999.
- [23] Shrout, Thomas R. and Chang, Zung P. and Kim, Namchul and Markgraf, Steven. Dielectric behavior of single crystals near the $(1-x)\text{Pb}(\text{Mg}_{1/3}\text{Nb}_{2/3})\text{O}_3 - (x)\text{PbTiO}_3$ morphotropic phase boundary. *Ferroelectrics Letters Section*, 12(3):63–69, 1990.
- [24] Yiping Guo, Haosu Luo, Di Ling, Haiqing Xu, Tianhou He, and Zhiwen Yin. The phase transition sequence and the location of the morphotropic phase boundary region in $(1-x)[\text{Pb}(\text{Mg}_{1/3}\text{Nb}_{2/3})\text{O}_3] - x\text{PbTiO}_3$ single crystal. *Journal of Physics: Condensed Matter*, 15(2):L77, 2003.
- [25] Xiaoning Jiang, Paul W Rehrig, Wesley S Hackenberger, Edward Smith, Shuxiang Dong, Dwight Viehland, Jim Moore Jr, and Brian Patrick. Advanced piezoelectric single crystal based actuators. In *Smart Structures*

- and Materials*, pages 253–262. International Society for Optics and Photonics, 2005.
- [26] Mickaël Thiercelin, Hichem Dammak, and Mai Pham Thi. Electromechanical properties of PMN-PT and PZT ceramics at cryogenic temperatures. In *Applications of Ferroelectrics (ISAF), 2010 IEEE International Symposium on the*, pages 1–4. IEEE, 2010.
- [27] FF Wang, WZ Shi, Siu Wing Or, XY Zhao, and HS Luo. Cryogenic transverse and shear mode properties of $(1 - x)Pb(Mg_{1/3}Nb_{2/3})O_3 - xPbTiO_3$ single crystal with the optimal crystallographic direction. *Materials Chemistry and Physics*, 125(3):718–722, 2011.
- [28] Xiaoning Jiang, William B Cook, and Wesley S Hackenberger. Cryogenic piezoelectric actuators. In *SPIE Optical Engineering+ Applications*, pages 74390Z–74390Z. International Society for Optics and Photonics, 2009.
- [29] Florian Martin, HJM ter Brake, Laurent Lebrun, Shujun Zhang, and Thomas Shrout. Dielectric and piezoelectric activities in $(1 - x)Pb(Mg_{1/3}Nb_{2/3})O_3 - xPbTiO_3$ single crystals from 5 K to 300 K. *Journal of Applied Physics*, 111(10):104108–104108, 2012.
- [30] Xiangyong Zhao, Bijun Fang, Hu Cao, Yiping Guo, and Haosu Luo. Dielectric and piezoelectric performance of PMNPT single crystals with compositions around the MPB: influence of composition, poling field and crystal orientation. *Materials Science and Engineering: B*, 96(3):254 – 262, 2002.
- [31] Robert E Newnham. *Properties of Materials: Anisotropy, Symmetry, Structure.*. Oxford University Press, 2004.
- [32] Zhang, Shujun and Xia, Ru and Shrout, Thomas R. Lead-free piezoelectric ceramics vs. PZT. *Journal of Electroceramics*, 19(4):251–257, 2007.

- [33] Gene H. Haertling. *Ferroelectric Ceramics: History and Technology*, pages 157–178. Wiley-VCH Verlag GmbH, 2007.
- [34] H Jaffe and DA Berlincourt. Piezoelectric transducer materials. *Proceedings of the IEEE*, 53(10):1372–1386, 1965.
- [35] B. Yurke, P.G. Kaminsky, and D.M. Eigler. Cryogenic piezoelectric displacement tester . *Cryogenics*, 26(7):435 – 436, 1986.
- [36] K Uchino. Materials issues in design and performance of piezoelectric actuators: an overview. *Acta Materialia*, 46(11):3745–3753, 1998.
- [37] D-S Paik, S-E Park, TR Shrout, and W Hackenberger. Dielectric and piezoelectric properties of perovskite materials at cryogenic temperatures. *Journal of materials science*, 34(3):469–473, 1999.
- [38] QM Zhang, Jianzhong Zhao, K Uchino, and Jiehui Zheng. Change of the weak-field properties of $Pb(ZrTi)O_3$ piezoceramics with compressive uniaxial stresses and its links to the effect of dopants on the stability of the polarizations in the materials. *Journal of materials research*, 12(1):226–234, 1997.
- [39] Seung-Eek Park and Thomas R. Shrout. Characteristics of relaxor-based piezoelectric single crystals for ultrasonic transducers. *IEEE Transactions on Ultrasonics, Ferroelectrics and Frequency Control*, 44(5):1140–1147, 1997.
- [40] F. Xu, S. Trolier-McKinstry, W. Ren, Baomin Xu, Z.-L. Xie, and K. J. Hemker. Domain wall motion and its contribution to the dielectric and piezoelectric properties of lead zirconate titanate films. *Journal of Applied Physics*, 89(2):1336–1348, 2001.
- [41] Matthew W. Hooker. Properties of PZT-Based Piezoelectric Ceramics Between -150 and 250C, 1998.